Atmos. Meas. Tech. Discuss., https://doi.org/10.5194/amt-2018-204
Manuscript under review for journal Atmos. Meas. Tech.
Discussion started: 5 July 2018

Atmospheric Measurement Techniques Discussions

Laser induced fluorescence based detection of atmospheric nitrogen dioxide and comparison of different techniques during the PARADE 2011 field campaign

Umar Javed[1,2], Dagmar Kubistin[1,3,4], Monica Martinez[1], Jan Pollmann[1], Markus Rudolf[1], Uwe Parchatka[1], Andreas Reiffs[1], Jim Thieser[1], Gerhard Schuster[1], Martin Horbanski[5], Denis Pöhler[5], John N. Crowley[1], Horst Fischer[1], Jos Lelieveld[1], and Hartwig Harder[1]

[1]Department of Atmospheric Chemistry, Max Planck Institute for Chemistry, Mainz, Germany
[2]Institute of Energy and Climate Research, IEK-8: Troposphere, Forschungszentrum Jülich GmbH, Jülich, Germany
[3]University of Wollongong, School of Chemistry, Wollongong, NSW, Australia
[4]German Meteorological Service, Meteorological Observatory Hohenpeissenberg (MOHp), Hohenpeissenberg, Germany
[5]Institute of Environmental Physics, University of Heidelberg, Heidelberg, Germany

Correspondence to: Hartwig Harder (hartwig.harder@mpic.de) or Umar Javed (u.javed@fz-juelich.de)

Abstract. GANDALF (**G**as **A**nalyzer for **N**itrogen **D**ioxide **A**pplying **L**aser-induced **F**luorescence), a new instrument for the detection of nitrogen dioxide based on the laser-induced fluorescence (LIF) technique, is presented in this paper. GANDALF is designed for ground based and air-borne deployment with a robust calibration system. In the current setup, it uses a multi-mode diode laser (447 – 450 nm) and performs in situ, continuous, and autonomous measurements with a laser pulse repetition rate of 5 MHz. The performance of GANDALF was tested during the field experiment at a forested location with urban influence where NO_x levels were between 0.12 and 22 parts per billion by volume (ppb_v). Based on the field results, the limit of detection is estimated at 5 – 10 parts per trillion by volume (ppt_v) in 60 s at a signal to noise ratio (SNR) of 2. The overall accuracy and precision of the instrument are better than 5 % (1 σ) and 0.5 % + 3 ppt_v (1 σ min^{-1}), respectively. A comparison of nitrogen dioxide measurements based on several techniques during the field campaign is presented to explore methodic differences.

1 Introduction

Tropospheric nitric oxide (NO) and nitrogen dioxide (NO_2) are key species in atmospheric chemistry and are strongly coupled due to their fast photochemical interconversion generally combined as NO_x (= NO + NO_2). Nitrogen oxides act as key catalyst in the formation of tropospheric ozone (O_3) (Crutzen, 1979). NO_x also plays an important role in the oxidation capacity of the troposphere by affecting the abundances of O_3, hydroxyl radical (OH), and nitrate radical (NO_3).

The main sources of NO_x in the troposphere are combustion processes, predominantly fossil fuel use, biomass burning, microbial production in soils, transport from the stratosphere and lightning, the latter two directly affecting the free troposphere [e.g. (Logan, 1983)]. NO_x emissions from the surface are mostly in the form of NO which is converted to NO_2 by the reaction of NO with O_3, the hydroperoxyl radical (HO_2), organic peroxy radicals (RO_2), and halogen oxides. The oxidation of nitrogen oxides in the atmosphere leads to the formation of several reactive nitrogen species, some of which act as reservoirs for NO_x, denoted by NO_z[1]. The NO_x lifetime is largely determined by its oxidation into nitric acid (HNO_3) by OH during daytime, and in polluted air also by the heterogeneous loss of N_2O_5 (formed by NO_2+NO_3) on wet surfaces during the night, e.g. on aerosols and cloud droplets. The tropospheric lifetime of NO_x is in the range of hours to days and it is generally shorter closer to the surface of

[1] NO_z = NO_3 + $2N_2O_5$ + HNO_3 + HONO + RO_2NO_2 + $RONO_2$ + HNO_4 + Particulate Nitrate + …

Atmos. Meas. Tech. Discuss., https://doi.org/10.5194/amt-2018-204
Manuscript under review for journal Atmos. Meas. Tech.
Discussion started: 5 July 2018

Earth compared to high altitudes [e.g. (Ehhalt et al., 1992)]. Because of its relatively short lifetime, the transport distance of NO_x is limited, compared to other primary pollutants like carbon monoxide (CO) and methane (CH_4) that disperse on hemispheric and global scales.

The wet and dry deposition of HNO_3 is considered the major sink for NO_x. Uncertainties in the NO_x budget have recently been highlighted (Stavrakou et al., 2013). These include the uncertainty in the estimate of the rate coefficient for NO_2 + OH under tropospheric conditions (Mollner et al., 2010), a lack of proper representation in chemical mechanisms for the loss of NO_x via organic nitrate formation (Browne and Cohen, 2012), and the formation of HNO_3 in a minor branch of the reaction between NO and HO_2 (Butkovskaya et al., 2007) which showed significant impacts on the concentration of NO_x, OH, HNO_3 and related chemistry (Cariolle et al., 2008;Gottschaldt et al., 2013). Additionally, a lack of agreement between modelled and measured OH concentrations over forests (Lelieveld et al., 2008;Kubistin et al., 2010) and urban regions (Hofzumahaus et al., 2009) contribute to uncertainty about NO_x chemistry. In summary, NO_x even in the low ppt_v range is important for understanding the tropospheric O_3 production (Lelieveld and Crutzen, 1990;Carpenter et al., 1997) and the cycling of radicals (Monks, 2005). Therefore, it is of great importance to have accurate NO_x measurements from regional to global scales.

Tropospheric mixing ratios of NO_x can vary from a few ppt_v to 100 ppb_v, depending on remote (Hosaynali Beygi et al., 2011) and urban conditions (Clapp and Jenkin, 2001), respectively. The high temporal and spatial variability of NO_x with the wide concentration ranges challenges its measurements. Briefly, several different methods have been used to measure NO_x in the atmosphere. The Photofragmentation Two-Photon Laser-Induced Fluorescence (PF-TP-LIF) in situ method was used in the past (Sandholm et al., 1990) to measure NO directly by using a spectroscopically selective laser to excite the molecule with subsequent fluorescence detection (Bradshaw et al., 1999). An indirect detection of NO_2 with this technique is also possible by converting $NO_2 \rightarrow$ NO via photofragmentation followed by NO detection. The $NO_2 \rightarrow$ NO photolytic conversion was performed using a XeF excimer laser at 353 nm (Sandholm et al., 1990) or Nd:YAG laser at 355 nm (Bradshaw et al., 1999). Whilst the PF-TP-LIF technique is adequate for an in principle interference-free detection of NO, the indirect detection of the NO_2 suffers from interferences originating especially from nitrogen containing species [e.g. (Crawford et al., 1996)]. The most common in situ method to measure NO_x is based on chemiluminescence detection. In this technique, the atmospheric NO reacts with an added excess amount of O_3 to produce electronically excited NO_2. The light intensity from the relaxation of electronically excited NO_2 is measured and proportional to the atmospheric NO (Fontijn et al., 1970). The chemiluminescence technique is arguably the best method available to measure NO directly because of better cost effective maintenance. This instrument is often combined with indirect NO_2 detection by converting it to NO. The $NO_2 \rightarrow$ NO conversion is either performed using a heated molybdenum catalyst or photolytic conversion. However, in the case of NO_2 to NO conversion, a potential interference from NO_z species cannot be fully excluded for the NO_2 measurement, e.g. (Villena et al., 2012;Reed et al., 2016). Therefore, a direct detection of NO_2 is advantageous. Techniques like cavity ring down absorption spectroscopy (Osthoff et al., 2006), tunable diode laser absorption spectroscopy (Herndon et al., 2004), cavity enhanced absorption spectroscopy (Wojtas et al., 2007), and cavity attenuated phase shift spectroscopy (Ge et al., 2013) provide direct in situ detection of NO_2. Another promising method for a direct NO_2 detection is based on the laser-induced fluorescence technique. The LIF method for NO_2 provides highly selective and sensitive measurements and it has already been demonstrated successfully in past with detection limits reaching down to about 5 $ppt_v\ min^{-1}$ (Thornton et al., 2000;Matsumoto and Kajii, 2003).

An overview of LIF NO_2 systems from the literature is given in Table 1. LIF systems have been used for many years but the detection limits are sometimes not suitable for detection in a remote region, especially in some of the earlier attempts (George and Obrien, 1991;Fong and Brune, 1997;Matsumoto et al., 2001;Taketani et al., 2007). In the last decade, owing to the advancements in lasers, better detection limits have been achieved. The LIF systems have shown good selectivity and sensitivity

Atmos. Meas. Tech. Discuss., https://doi.org/10.5194/amt-2018-204
Manuscript under review for journal Atmos. Meas. Tech.
Discussion started: 5 July 2018

(Thornton et al., 2000;Matsumi et al., 2001;Matsumoto and Kajii, 2003;Dari-Salisburgo et al., 2009), but most of these systems have large (typically > 50 kg) and complex laser systems. The availability of much smaller and lighter diode lasers have made it possible to build compact instruments with the caveat of lower laser power and higher detection limits. Here for GANDALF, a high power, lightweight diode laser (< 2 kg) system is used to achieve a compact design with detection limits comparable to those of the best performing larger instruments.

In the following the newly developed LIF instrument for the direct NO_2 detection is described. Results from the first field deployment in a semi-rural region are reported to demonstrate the performance of the instrument. Measurements of trace gases along with meteorological parameters were carried out during the campaign, including NO_2 measurements based on several techniques, namely LIF, cavity ring down absorption spectroscopy, two-channel chemiluminescence detection, cavity-enhanced differential optical absorption spectroscopy, and long-path differential optical absorption spectroscopy. Being the first deployment of GANDALF, this opportunity provided the means for a detailed comparison to other methods under real atmospheric conditions.

2 The instrument description

2.1 The operational method

The measurements of GANDALF are based on laser-induced fluorescence at low pressure (<10 hPa). The NO_2 molecule is excited by a diode-laser with a wavelength well above the photolysis threshold (λ > 420 nm for NO_2) and the red-shifted fluorescence is detected during laser-off periods.

$$NO_2 + h\upsilon\ (\lambda = 449nm) \rightarrow NO_2^* \qquad R.\ 1$$

$$NO_2^* \rightarrow NO_2 + h\upsilon' \qquad R.\ 2$$

The detected fluorescence $h\upsilon'$ is directly proportional to the amount of NO_2 in the cell. The background signal due to scattering and dark counts of the detector are determined by frequently measuring zero air. The atmospheric mixing ratios of NO_2 are derived by using Eq. 1.

$$NO_2 = \left[\frac{Signal - S_{BG}}{\alpha_c}\right] \qquad Eq.\ 1$$

Where 'Signal' is in counts s^{-1} and α_c is the calibration factor or sensitivity in counts s^{-1} ppb^{-1}. α_c is derived from the slope of counts versus known amounts of NO_2. 'S_{BG}' is the background signal in counts s^{-1}. The quality of zero air is further discussed in section 3.

The mechanical and optical parts of the LIF detection axis are presented schematically in Fig. 1. All mechanical parts inside GANDALF are black anodised and most optical components (Fig. 1, no.12) are continuously flush with zero air (3 × 50 sccm) during the period of operation to avoid dead air pockets, fog, dust, etc. The inlet for the sampling flow is a small orifice with a diameter of 0.7 mm. The distance from the point of entrance at the orifice to the centre of the detection cell is about 150 mm. This combination of orifice size and scroll pump provides a pressure of 7 hPa inside the detection cell, with a sampling

flow of about 4100 sccm. The time required for air molecules from the point of entrance to reach the centre of the detection cell is less than 30 ms. The **diode laser**[2] in this system has a maximum output power of 250 mW with an on-off modulation frequency of 5 MHz. The wavelength (λ) of the diode laser is in the range of 447 → 450 nm. The convolution of the laser profile and the NO_2 absorption cross-section (Vandaele et al., 2002) yields an effective NO_2 absorption cross-section of 5.3×10^{-19} cm^2 $molecule^{-1}$. A **Herriot cell** (Herriott et al., 1964) is used to produce multiple passes to enhance the laser light, and focus at the centre of the detection cell. The detection cell of GANDALF is positioned between the Herriott cell mirrors, which have approximately 99.99 % reflectivity (IBS coating)[3] in the spectral range of 445 nm to 455 nm. The distance between the mirrors is twice their radius of curvature (R = 128 mm). Any fluorescent contaminants from the mirrors is measured as a part of the background signal. The laser beam is directed (Fig. 1, no.4) into the detection cell by using motorised mirrors. These mirrors are coated to achieve high reflectivity (99.8 %) for a light incidence at 45° with a wavelength of 450 nm. The multi-passed laser beam encompass a circle of about 8 - 10 mm diameter at the centre of the detection cell. A **photon counting head**[4] (PMT) is used for the fluorescence detection. The PMT is located in a tube perpendicular to the sampling flow. The effective sensor area of the PMT is 5 mm in diameter and has a GaAsP / GaAs photocathode[5]. The PMT is sensitive to wavelengths between 380 nm and 890 nm, with peak sensitivity at 800 nm with a maximum quantum efficiency of 12 %. The fluorescence signal is focused onto the PMT by collimating lenses (Fig. 1, no. 9). An aluminium concave mirror (Fig. 1, no.7) located opposite of the PMT redirects additional fluorescence photons towards the detector. In front of the PMT, **interference filters**[6] (Fig. 1, no.10) are used to remove contributions of light scattered from the walls of the sampling chamber, as well as from Rayleigh and Raman scattering. The filters have the cut-off wavelength (block radiation below this wavelength) of 470 nm and 550 nm respectively, with an average transmission of 98 % in the spectral range from cut-off wavelength + 3 nm to 900 nm. The reflectivity of the filters is higher than 99.7 % for the spectral ranges of about 8 nm below the cut-off wavelengths. The filters have a very small (< <1 %) absorption for almost the entire spectral regimes. However on the edge of the photonic stop band (cut-off wavelength) the absorption can be up to 7 % and 4 % for the filters with cut-off wavelength of 470 nm and 550 nm, respectively. At this positon, the photon density reaches to its maximum which increases the probability of absorption of a photon. If this absorption at about the cut-off wavelength exist than this can potentially amplify the luminescence. The fluorescence contamination is corrected using the background signal measurements. An optical system (Fig. 1, no.3) based on photodiodes and a NO_2 filled cuvette is installed to monitor the change in the wavelength and power of the diode laser. The stray light in the system is reduced to a minimum by using a combination of baffles. There are different types of baffles (Fig. 1, no.11 and 13) used in the system to reduce scatter from walls or mirrors. The shape of a baffle surface is based on a zigzag pattern with a 30° angle. The sharpened edges of a baffle provide less surface area for the laser light to scatter and have the characteristics of a light trap. The surface of the diode laser and PMT are continuously kept at a constant temperature by a circulated water chiller.

The diode laser has a 'Deepstar' mode, which is used as an advantage for the system. While operating in this mode with the repetition rate of 5 MHz, there is no laser radiation during the off period and the NO_2 fluorescence is detected during the laser off period. To determine the optimum sensitivity as a function of the repetition range, the relative NO_2 fluorescence intensities for different on-off cycles has been calculated by taking into account key parameters like NO_2 absorption cross-section, pressure, flow velocity, fluorescence lifetime, and the power of the diode laser. The calculated sensitivity for different laser on-durations is

[2] Omicron Laserage (CW Diode-Laser), laserproduckte GmbH, Germany
Power stability <1 % $hour^{-1}$, pointing stability: <10μrad
Beam diameter: 2.55 (perpendicular: 0°/mm) & 2.53 (parallel: 90°/mm)
[3] ATFilms (IBS coating), USA
[4] Hamamatsu (H7421-50), Japan, Count sensitivity: 2.1×10^5 $s^{-1}pW^{-1}$ at 550 nm and 3.9×10^5 $s^{-1}pW^{-1}$ at 800 nm
[5] Radiant sensitivity of 87.4 mA W^{-1}
[6] Barr Associates, Inc., USA

shown in Fig. 2 based on 1 ppb_v of NO_2 as a function of off-period duration. For a comparison to current operational on-off cycles, three different on-periods are shown in Fig. 2. The best sensitivity of the instrument is achievable by operating the diode laser at 5 MHz, 100 ns on, 100 ns off. The time-resolved raw signal (both on-off cycle) are stored in 4 ns bins (4 ns bin = 1 channel) for a specified time of integration (typically 1 s). For the total fluorescence signal 20 of these channels are summed up and used as a signal for NO_2. The first 5 channels or 20 ns of the laser off period are ignored because these channels still contain some scattered light signals from the laser light and walls of detection cell.

2.2 Calibration system

The LIF method is not an absolute technique and requires calibration. The sensitivity (Eq. 1) of GANDALF depends on e.g. background noise, laser power or wavelength, temperature, pressure, residence time in the sampling line, etc. It is determined using NO_2 concentrations generated by gas phase titration of NO to NO_2 by means of O_3 (R. 3). Using commercial available NO_2 gas cylinders at low concentrations (Thornton et al., 2000;Dari-Salisburgo et al., 2009), was not chosen due to its open questions with its long term stability at low concentration. The calibration system is described in the following sections.

The NO calibration mixture for the gas phase titration is traceable to a primary NIST[7] standard (4.91 ± 0.04 µmol mol^{-1} in nitrogen). The overall uncertainty of the NO calibration mixture is 2 %. NO is almost completely (> 98 %) consumed during gas phase titration with O_3 in the calibrator. This is achieved by using a high concentration (> 1.4 ppm_v) of O_3. NO_2 also reacts with O_3 to form NO_3 (R. 4). The reaction of NO_2 with O_3 (R. 4) is slower by 3 orders of magnitude compared to the reaction of NO with O_3 (R. 3), with a reaction rate of 3.5×10^{-17} cm^3 $molec^{-1}$ s^{-1} compared to 1.8×10^{-14} cm^3 $molec^{-1}$ s^{-1} at 298 K (Atkinson et al., 2004), respectively. However, at higher concentrations and due to the long residence times, the reaction between NO_2 and O_3 can become important, leading to a loss of NO_2 generated in the calibrator with subsequent losses due to further reaction between NO_2 and NO_3 (R. 5).

$$NO + O_3 \rightarrow NO_2 + O_2 \qquad \text{R. 3}$$

$$NO_2 + O_3 \rightarrow NO_3 + O_2 \qquad \text{R. 4}$$

$$NO_2 + NO_3 + M \leftrightarrow N_2O_5 + M \qquad \text{R. 5}$$

Numerical simulations are used to assess the optimum setup for the calibration device by studying the impact of different parameters like concentrations levels, residence time, flow rates, pressure, etc. Based on box model (BM) simulations and verified by lab experiments, a PFA (Perfluoroalkoxy) reaction chamber for the completion of the gas phase titration between NO and O_3 has been designed to achieve maximum conversion efficiency for $NO \rightarrow NO_2$. The BM simulation is shown in Figure 3 Fig. 3 for typical calibration parameters[8]. The mixing ratios of NO, O_3, and NO_2 are plotted as a function of residence time in the left panel of Fig. 3. This simulation predicts that more than 99 % of NO is converted to NO_2 within the residence time

[7] National Institute of Standards and Technology, USA
[8] For this specific simulation, initial parameters;
NO = 5 sccm × 10.55 ppm_v,
O_3 = 500 sccm × 1.7 ppm_v,
residence time in the reaction chamber = 7.5s,
flow = 8000 sccm
temperature and pressure = 298 K and 1013.25 hPa

of 7.5 s inside the reaction chamber. The formation of NO_3 and N_2O_5 in the reaction chamber is negligible (< 0.5 ppb_v) compared to NO_2 (> 100 ppb_v). The formation of NO_3 and N_2O_5 can thus only raise < 1 % uncertainty in the generated NO_2 for typical operating conditions of the calibrator. After the reaction chamber, the calibration gas mixture is further diluted with zero air to achieve a required range (close to ambient levels) of NO_2 mixing ratios.

The calibration system was tested for different concentrations of O_3. Figure 4 shows the NO_2 signal of the PMT (after dilution of the calibration gas) based on different O_3 mixing ratios in the reaction chamber for a constant NO concentration (about 0.1 ppm_v). For O_3 concentrations below 1 ppm_v non stoichiometric conversion of NO was observed as expected. The PMT signal reached a maximum at about 1.356 ppm_v and this signal is explained by the derived NO_2 concentration from the BM simulation. The decrease of the PMT signals at higher O_3 concentrations above 1.4 ppm_v mainly due to loss of NO_2 in reactions R. 4 and R. 5. The amount of NO_2 generated in the 'NO + O_3' titration is much less sensitive to O_3 than to NO as losses of NO_2 (R. 4) also being dependent on O_3 for the chosen parameters. If O_3 is increased by 1 ppm_v above the optimum mixing ratio of 1.3 ppm_v (Fig. 4), NO_2 is reduced by only 1 %. The O_3 concentrations are always kept above this threshold limit and the concentrations are measured using an O_3 analyser[9] with a typical precision of 5 %. Above the threshold, a 5 % change in O_3 produces an uncertainty in NO_2 of less than 0.5 %.

A NO_x analyser[10] was used to determine the remaining concentrations of NO inside the calibrator after the gas phase titration. About 99 % of NO is consumed in the gas phase titration for most of the cases at O_3 > 1.4 ppm_v. There are two different regimes in the calibration system based on different NO and O_3 concentrations and different flow rates: (1) gas phase titration in the reaction chamber and (2) dilution with zero air after the reaction chamber. Considering the flow rates and dimensions of the gas lines, the theoretically calculated total residence time based on the plug flow assumption is 7.73 s. While the total residence time for the calibration gas in the calibration system is also determined experimentally by using Eq. 3.

$$NO_{GPT} = D[NO_i]\left(e^{-k_{R.3}[O_3]t_1}\right)\left(e^{-k_{R.3}[O_3]Dt_2}\right) \quad \text{Eq. 2}$$

$$\Rightarrow [t_1 + Dt_2] = -\left[\frac{ln\left(\frac{NO_{GPT}}{D[NO_i]}\right)}{k_{R.3}[O_3]}\right] \quad \text{Eq. 3}$$

In Eq. 3, 'NO_{GPT}' is measured with the NO_x analyser and is defined as the NO concentration remaining in the calibration gas after the gas phase titration and dilution. $[NO_i]$ is the initial concentration of NO before the gas phase titration. 'D' is the dilution factor after the reaction chamber. 't_1' is the residence time for the reaction chamber and 't_2' is the dilution dependent travel time for a NO_2 molecule from the exit of the reaction chamber to the inlet of GANDALF. $[O_3]$ in Eq. 3 is the concentration in the reaction chamber. '$k_{R.3}$' is the temperature dependent rate coefficient for R. 3. There are two slightly different (< 6% based on rate constant at 298K) values reported in the literature for the temperature dependent $k_{R.3}$ as follows:

$$k_{R.3} = 3 \times 10^{-12} \times e^{\left(\frac{-1500}{T}\right)} \qquad (1.9 \times 10^{-14} cm^3 molec^{-1} s^{-1} \; at \; 298K) \qquad \text{(Sander et al., 2011)}$$

$$k_{R.3} = 1.4 \times 10^{-12} \times e^{\left(\frac{-1310}{T}\right)} \qquad (1.8 \times 10^{-14} cm^3 molec^{-1} s^{-1} \; at \; 298K) \qquad \text{(Atkinson et al., 2004)}$$

[9] ANSYCO, O3-41M, 'Analytische Systeme und Componenten GmbH', Germany
[10] Model: ECO PHYSICS CLD 780 TR, Switzerland

Based on Eq. 3, the average value of total residence time [t_1 + D t_2] is 7.32 s ± 0.25 s (Sander et al., 2011) or 8.38 s ± 0.29 s (Atkinson et al., 2004) as shown in Fig. 5. The estimated accuracy of these two values for the total residence time is 6.5 % (1σ).

The temperature and pressure also affect the formation of NO_2 inside the reaction chamber, and these effects were tested with the box model. In the simulations all parameters except temperature or pressure are kept constant. At a lower temperature the reaction between NO and O_3 slows down leading to changes in the conversion efficiency from NO to NO_2. According to the box model simulations temperature variations within 5 - 45 °C leads to an overall relative uncertainty of 1 % (1σ) for the whole range. Similarly, the impact on the calibration gas due to a change in the atmospheric pressure is not significant. Based on the box model simulations, the relative uncertainty in the NO_2 concentration of calibration gas due to a change in the atmospheric pressure over an interval of 800 – 1013 hPa is below 0.5 % (1σ).

The calibration gas for GANDALF primarily contains N_2 (~79.5 %) and O_2 (~20.5 %) with H_2O vapour (< 25 ppm_v). The level of H_2O vapour in the atmosphere can reach up to about 3 % (Seinfeld and Pandis, 2006). The sensitivity of the instrument is reduced by atmospheric H_2O vapour because collisions with H_2O molecules quench the NO_2 fluorescence. The H_2O dependency is evaluated experimentally by diluting the calibration gas with known amounts of water vapour concentrations and its effect on sensitivity during field measurements is corrected by using simultaneous measurement of H_2O vapour in the atmosphere. The H_2O concentrations during calibration are determined using an existing calibration system for the LIF-OH instrument (Martinez et al., 2010). The decrease in the sensitivity for GANDALF is 5 % ± 1 % (1σ) at 1 % of atmospheric H_2O vapour.

A robust calibration system has been developed for the automated calibration of the instrument. GANDALF is frequently calibrated (up to 8 times in 24h) during field operations to track changes in sensitivity. An example for a calibration plot is shown in Fig. 6. The calibration system is controlled by Mass Flow Controllers (MFC)[11] and electronic valves[12]. All MFC are calibrated using a DryCal[13] sensor which is traceable to a NIST standard (NIST traceability is confirmed by Westphal[14]). The uncertainty in the set flows, based on a certified value, is 1 % (level of confidence 95 %). O_3 is generated for the calibration using an ozone generator[15]. Different NO_2 mixing ratios are achieved by changing the NO flow (range up to 10 sccm), while the O_3 concentration (> 1.4 ppm_v) and flow (500 sccm) are kept constant. Figure 7 shows a schematic of the setup for the automated calibration procedure of GANDALF. A small pump (Cal. pump) is connected to the main sampling line of GANDALF. A three-way electronic valve (EV2) and a manual needle valve (MNV) are attached in front of the calibration pump. To minimise any line effects such as a decomposition of species like PAN, the chemical reaction of the ambient NO and O_3, etc., the residence time in the sampling line is kept at less than 0.1 s by a flow ≥ 10000 sccm required during ambient air measurements. GANDALF has a flow of 4100 sccm through the pin hole and the rest of the flow is diverted to the main exhaust by the calibration pump. The amount of total sampling flow can be increased or decreased by adjusting the manual valve MNV.

During ambient air measurements, valve EV2 is opened for line L1 (shown in green in Fig. 7) and allows an extra flow of about 8000 - 9000 sccm to pass from the sampling flow to the calibration pump (direction shown by the white arrow in Fig. 7). Line L1 is simultaneously used to condition the NO calibration line with a flow of 2 sccm NO gas, which goes directly to the exhaust without entering the measurement cell.

Frequent zero-air measurements are necessary to monitor changes in the background signal of GANDALF. A four-way electronic valve (EV3) and a mass flow controller (MFC Zero) are used to switch the zero air background flow (8000 sccm) on

[11] MKS Instruments and Bronkhorst HIGH-TECH B.V, USA
[12] Solenoid Operated Diaphragm, Galtek, USA
[13] DC-2, BIOS International Corporation , USA
[14] WESTPHAL measurement and control technique GmbH & Co. KG, Germany
[15] SOG2, 185nm, UVP - Ultraviolet Products, USA

and off in line L3. During background signal measurements, an excess of zero-air about 3900 sccm (blue arrow in Fig. 7) is diverted to the calibration pump through line L1 by setting the valve EV2 to position P1, along with about 5100 sccm flow of ambient air.

During calibration the zero air flow is switched on and used for dilution of the calibration gas. Line L1 is closed and instead line L2 is opened by valve EV2 to remove the calibration gas overflow of 3900 sccm together with 5100 sccm from the ambient (illustrated by the red arrows in Fig. 7). For the gas phase titration, the flow of O_3 is switched on and off by the two-way electronic valve EV1 and MFC (O_3). The flow of NO (1 - 10 sccm) is controlled by a mass flow controller [MFC (NO) in Fig. 7]. Since all overflows are diverted to an exhaust, this setup allows frequent checks of the GANDALF sensitivity and background signal without disturbing the ambient conditions for a nearby operating instrument. Based on calibrations during PARADE-2011, the repeatability of the sensitivity was 2.7 % (1σ), with an overall uncertainty of the calibration system of approx. 5 % (1σ).

2.3 Precision and limit of detection

The precision of the instrument was evaluated by using a set of randomly chosen individual calibrations from the field experiment (PARADE-2011). The relative precision of GANDALF for these calibrations is shown in Fig. 8. The relative precision on the randomly selected calibration data points was better than 0.5 % (1 σ at 1 min integration time) for most of the data points despite a few outliers (Fig. 8). For an overall precision of GANDALF, an absolute value of < 5 ppt_v (1σ) has to be added to the relative precision. This absolute value arises from the variability in the zero-air signal and is derived from the intercept of a fit of absolute precisions of calibration points during PARADE versus mixing ratios of NO_2. The variations in background signal for GANDALF is proportional to the square root of the integration time. These variations around an average background signal measured with zero-air dominate the precision of the instrument close to the detection limit.

The precision of the instrument background signal was also cross-checked using a continuous measurement of zero-air for about 50 minutes. In order to verify the square root dependency of the signal variability on integration time, an Allan deviation plot is used (Riley, 1995;Land et al., 2007). Figure 9 shows an overlapping (Riley, 2008) Allan deviation plot of variations in background signal versus averaging time. The variations in background signal with a 60 s integration time are equivalent to an absolute NO_2 value of about 3 ppt_v (1σ). Figure 9 also shows that the random noise of the instrument background signal can be reduced by averaging, with a square root dependency on time, at least up to a 60 s period. The background signal of GANDALF is frequently checked during a field operation (e.g. during PARADE, 1 background signal measurement per hour).

The limit of detection (LOD) can be derived from the variation of the background signals. Based on the Allan deviation plot in Fig. 9, a limit of detection of about 3 ppt_v (1σ) NO_2 for one minute averaged measurements is expected. The stated (Table 1) LOD of GANDALF was calculated using Eq. 4 (Taketani et al., 2007) at a signal-to-noise ratio SNR of 2 and considering the two times higher background signal.

$$LOD = \frac{SNR}{\alpha_c}\sqrt{\frac{2\times S_{BG}}{t}} \qquad \text{Eq. 4}$$

Where α_c is the calibration factor or sensitivity in counts (s^{-1} ppb^{-1}), S_{BG} is the background signal in counts (s^{-1}) and t is the averaging time in seconds. The LOD for GANDALF, based on sensitivity and background measurements during the field experiment (PARADE-2011), varied between 5 and 10 ppt_v.

Atmos. Meas. Tech. Discuss., https://doi.org/10.5194/amt-2018-204
Manuscript under review for journal Atmos. Meas. Tech.
Discussion started: 5 July 2018

295 **2.3 Interferences by other species**

Several atmospheric gas species can absorb the 449 nm laser light inside the detection cell. This can lead to interference for the NO_2 measurements with GANDALF directly (photodissociation process) or indirectly (fluorescence).

Iodine monoxide (IO) has an absorption cross-section of 3.9×10^{-18} cm^2 $molecule^{-1}$ (Harwood et al., 1997) and is about 8 times higher than NO_2 at 449 nm. Even a few ppt_v of IO in the atmosphere can produce a significant fluorescence signal,
300 especially in the marine atmosphere for which IO is mostly reported (Commane et al., 2011) . The fluorescence lifetime of IO is only 1-10 ns (Bekooy et al., 1983;Newman et al., 1998). As described earlier, the initial 20 ns fluorescence signal is ignored in the GANDALF data evaluation. So the IO fluorescence signal after 20 ns becomes too small to significantly interfere with the NO_2 fluorescence signal.

Nitrogen containing inorganic species (NO_3, N_2O_5, $HONO_2$, HO_2NO_2, PAN, ClONO, $ClNO_2$, and $ClONO_2$) can produce
305 NO_2 by photodissociation which can happen inside the detection cell. N_2O_5 (Harwood et al., 1993), $HONO_2$ (Burkholder et al., 1993), HO_2NO_2 (Singer et al., 1989), PAN (Talukdar et al., 1995), and ClONO (Molina and Molina, 1977) are not known to photo-dissociate at this wavelength. The absorption cross-sections for $ClONO_2$ (Molina and Molina, 1979) and $ClNO_2$ (Ghosh et al., 2012) are smaller by about 4 orders of magnitude compared to that of NO_2 at 449 nm. The tropospheric concentrations of $ClONO_2$ and $ClNO_2$ are generally smaller to similar compared to ambient NO_2. Hence, an interference from these species is
310 highly unlikely.

NO_3 has a larger absorption cross-section (Wayne et al., 1991) at 449 nm compared to the previously described nitrogen-containing species. The effective absorption cross-section, calculated from (Wayne et al., 1991), is about a factor of 2 smaller than that of NO_2 at the wavelength of the diode laser. The recommended quantum yield for the photodissociation of NO_3 to NO_2 + O is about 1 at wavelengths below 585 nm (Sander et al., 2011); hence, its fluorescence (Wood et al 2003) is
315 insignificant compared to its photodissociation to NO_2. Interference from photodissociation of NO_3 is therefore a two-photon process:

$$NO_3 + h\upsilon_{DiodeLaser} \rightarrow NO_2 + h\upsilon_{DiodeLaser} \rightarrow NO_2^* \rightarrow NO_2 + h\upsilon \qquad \text{R. 6}$$

320 The lifetime of NO_3 can be estimated from Eq. 5.

$$\tau(NO_3) \approx \int \sigma_{NO_3}(\lambda, T) \times \varphi_{NO_3}(\lambda, T) \times F(\lambda, T)\, d\lambda \qquad \text{Eq. 5}$$

Where σ (λ, T) is the effective absorption cross-section of NO_3 which is 2.7×10^{-19} cm^2 $molecule^{-1}$; φ (λ, T) is the quantum yield
325 for NO_3, and F (λ, t) is the photon flux from the diode laser of about 10^{20} photons cm^{-2} s^{-1}. The residence time of sampling air in the effective beam area of the laser is much smaller (<0.001 s) compared to the NO_3 photodissociation lifetime (> 0.01 s). Due to this reason, any chance of a significant interference from the NO_3 photodissociation is highly unlikely. Moreover, the ratio of the atmospheric concentration between NO_2 and NO_3 is very high, e.g. during PARADE the median ratio NO_2 / NO_3 was 430 for NO_3 > 0 with a minimum value of 12.

330 Alkenes and aromatics (aldehydes and benzene) are also abundant in the troposphere. However, absorption of alkenes and aromatics occurs in the UV range (< 300 nm) (Keller-Rudek et al., 2013), well below the wavelengths used in GANDALF. Some carbonyls like glyoxal (CHOCHO), and methylglyoxal (CH_3COCOH) also have absorption in the blue region of the

visible spectrum. The absorption cross-section values of CHOCHO, and CH3COCOH are 5.28 $\times 10^{-20}$ cm^2 $molecule^{-1}$ (Horowitz et al., 2001), and 9.26×10^{-20} cm^2 $molecule^{-1}$ (Meller et al., 1991;Staffelbach et al., 1995) at 449 nm, about a factor 10 and 5 smaller than the NO_2 absorption cross-section, respectively. Also the fluorescence from these species is not known to be present in the region of NO_2 fluorescence. So, the interference from these species is not important.

To minimise the impact of heterogeneous or thermal conversion of species like PAN, HO_2NO_2 and N_2O_5 yielding NO_2, a short residence time of < 0.1 s is generally used by keeping the sampling flow high, e.g. 12000 sccm in a 0.5 m long sampling line with a 4 mm internal diameter during PARADE-2011. An intercomparison of GANDALF and other measurements of NO_2 during PARADE-2011 was conducted to look for systematic dependencies of the differences between the different measurements on several measured atmospheric quantities. No evidence for a potential interference has been found for GANDALF (Section 3.2).

3 Field Experiment: PARADE-2011

The PARADE, **PA**rticles and **RA**dicals: **D**iel observations of the impact of urban and biogenic **E**missions, field experiment took place at the Taunus Observatory on Kleiner Feldberg (825m ASL[16]; 50.22° N, 8.45° E) in Germany from the 15th of August (DOY[17] = 226) to the 10th of September (DOY = 252) 2011. The general focus of PARADE was to characterise summertime biogenic emissions and photochemistry in a forested environment with anthropogenic influence. The observatory is located in the vicinity of the Taunus region at the hilltop of Kleiner Feldberg. A total area of 5 km radius around the observatory is dominated by coniferous, broad leaved and mixed forest. The measurement platform was located at the top of the observatory. The site is often affected by anthropogenically influenced air from nearby cities such as Frankfurt/Main (30 km SE), Wiesbaden (20 km SW), Mainz (25 km SSW), and some roads within 5 - 10 km, depending on the wind direction. The temperature during PARADE varied within a range of 5 - 28 °C with an overall average of 14.8°C. The temperature conditions during PARADE can be subdivided into two phases. The periods of DOY = 226 - 237 and DOY = 243 - 246 for PARADE were slightly warmer and the temperature mostly stayed above 15 °C, whereas during the other periods of DOY = 238 - 242 and DOY = 248 - 252 the temperature was below 15°C. The relative humidity (RH) had an overall average value of 77 % and variations within the interval of 37-100 %. There were several episodes of rain during PARADE. In the later part of the campaign, fog persisted in the early morning hours. Air masses at the observatory arrived predominantly from the southwest (SW) to the northwest (NW) side of Kleiner Feldberg. Sampling lines for most of the trace gas monitoring instruments were located within a 5 m^2 area at the top of the platform. The platform was about 8 m above ground and the top of the platform was above the forest canopy. An overview of the instrumentation and conditions during PARADE can be found e.g. in (Phillips et al., 2012;Bonn et al., 2014). Note that all data sets for analysis are based on available 10-minute averages.

3.1 NO_2 inter-comparison during PARADE

NO_2 concentrations were measured with eight different instruments. Six out of eight instruments sampled at the top of the platform. The measurement techniques, uncertainties, time resolutions and LOD are summarised in Table 2 for the instruments located on the platform. The average ambient concentrations of NO_2 during PARADE were approx. 2 - 3 ppb_v with a range of

[16] above sea level
[17] DOY (Day of year 2011)

approx. 0.13 ppb_v to 22 ppb_v. NO_2 instruments listed in Table 2 represent in situ measurement techniques with the exception of the LP-DOAS (Long Path Differential Optical Absorption Spectroscopy).

A median value (based on 10 minute averages) of the atmospheric NO_2 concentration is derived from the NO_2 measurements of all individual instruments at the platform including LP-DOAS. For a valid correlation between the derived median NO_2 and individual NO_2 measurements, only those values of the median NO_2 were selected for which simultaneous data for all NO_2 measurements were available. Figure 10 shows the correlation between individual NO_2 measurements and the derived median NO_2 concentrations. The total uncertainties of individual instruments are shown as error bars on the y-axis while horizontal bars represents the standard deviation of the derived median NO_2. The regression is done by using a 'bivariate' fit according to the method described in (York et al., 2004;Cantrell, 2008).

LP-DOAS: This instrument is based on traditional Differential Optical Absorption Spectroscopy (DOAS) (Platt et al., 1979;Perner and Platt, 1979), and follows the Beer-Lambert law. DOAS allows direct and absolute measurements of multiple trace gases in the atmosphere by using the distinct absorption band structure of the specific molecule (i.e. calibration is not needed) (Platt and Stutz, 2008). LP-DOAS is based on active remote sensing and requires an artificial light source (Pöhler et al., 2010). It provides an average concentration of NO_2 or other trace gases through quantitative detection using the absorption over a light path of typically a few kilometres. The instrument in this study is a well-established instrument and has been a part of many field campaigns (Pöhler et al., 2010). During PARADE, the optical path length was approximately 2.5 km and the light source as well as the spectrograph was located on the platform. The optical retro-reflector reflecting the light back to the telescope was located on the mountain Großer Feldberg (Distance =1.23 km and Height = 37 m). Therefore the LP-DOAS measurement delivers values integrated along a 1.2 km straight line starting at the platform to the retro-reflector. The correlation ($R^2 = 0.96$) plot between LP-DOAS and the derived median NO_2 values is shown in subplot E of Fig. 10. The slope of the fit is 1.02 ± 0.005 with a negligible y-intercept of -0.002 ± 0.009 ppb_v and these values are within the uncertainty of the instrument. The uncertainty of LP-DOAS is mainly due to errors in the absorption cross-sections of NO_2. A larger scatter between the LP-DOAS to the in situ instruments is expected due to the sampling of different air masses (A1 in Fig. 11).

CE-DOAS: Cavity-Enhanced DOAS (Platt et al., 2009) measurements of NO_2 were also available during PARADE. This method is based on Differential Optical Absorption Spectroscopy (DOAS) combined with a cavity and provides in situ measurements of trace gases (Platt et al., 2009). CE-DOAS requires calibration of the absorption light path in the cavity. This was performed with the measurement of two different Rayleigh absorbers (Helium, and air) according to (Washenfelder et al., 2008). The campaign was also the first field trial for this instrument with a reported error of measurements in the range of 5 – 10 %, mainly due to the accuracy of the light path calibration. The CE-DOAS and the CRDS shared the same sampling line. The slope and the y-intercept for CE-DOAS versus the median derived NO_2 is 0.92 ± 0.007 and -0.032 ± 0.01 ppb_v, respectively, with $R^2 = 1$ as shown in subplot [F] of Fig. 10. The difference to the median value is well within the range of instrumental uncertainty of this prototype.

CRDS: Besides the DOAS instruments, another NO_2 measurement technique using a Cavity Ring-Down Spectrometer (CRDS) was available (Thieser et al., 2016). CRDS is a cavity-assisted method like CE-DOAS (Platt et al., 2009). It is a direct method for in situ measurements which requires no calibration but only the background (zero-air) measurements. In CRDS, reflective mirrors are used across an optical cavity. To obtain the concentration of a trace gas with CRDS, absorption measurements to determine the time constant for exponential decay of the light intensity with and without an absorber are made in the optical cavity. During PARADE, the instrument inlet was located 2 m above the platform. An about 8 m long PFA tube was used for the sampling air. The slope and y-intercept in the case of CRDS are 1.06 ± 0.007 and 0.01 ± 0.01 ppb_v with correlation $R^2 = 0.99$ as shown in panel D of Fig. 10. The reported upper limit of uncertainty in the case of CRDS is

[6 % + 20 ppt_v + (20 ppt_v × RH[18] /100)] (Thieser et al., 2016). The differences between CRDS and the derived median NO_2 values are smaller than the instrument errors.

CLD/Blue-light converter (BLC): Along with the above mentioned absolute methods, the concentrations of NO_2 and NO were determined with a two-channel chemiluminescence detector (CLD). The instrument sampled air via ~8 m long PFA tubing at 2 m above the platform. The CLD instrument of MPIC is well-established, being an improved version (Hosaynali Beygi et al., 2011) of the ECO-Physics CLD 790 SR. In this instrument, NO_2 is detected by conversion via photolysis to NO, using a blue light converter at the wavelength of 395 nm, with subsequent detection of NO by chemiluminescence. The calibration of the system is done by using gas phase titration between NO and O_3 to produce stoichiometric quantities of NO_2. The correlation (R^2 = 0.99) between CLD and the derived median NO_2 values is shown in panel C of Fig. 10. Overall, the data of the CLD is about 5 % below the median, but this difference is within the uncertainty of the CLD measurement. The reported uncertainty of the CLD for the NO_2 measurements is 105 ppt_v or 10 % (Li et al., 2015). The slope and y-intercept are 0.95 ± 0.008 and − 0.1 ± 0.01 ppb_v, respectively. A larger negative intercept could be related to measurements of higher background for the BLC unit (switch ON) leading to underestimation of ambient NO_2. An additional background signal is most likely due to decomposition of surface absorbed NO or NO_2 during the operational mode of the BLC unit (Teflon block).

GANDALF: The sampling flow rate (12000 sccm) provided a residence time of less than 0.1 s in a 0.5 m sampling line. This was sufficient to suppress the impact of heterogeneous or thermal conversion of NO_2 containing species to yield NO_2. The formation of NO_2 due to the reaction between ambient NO and O_3 in the sampling line was negligible. The campaign averages of the observed concentrations of NO, O_3 and NO_2 were 0.25 ppb_v, 44 ppb_v and 2.6 ppb_v respectively. Based on average NO and O_3 concentrations, the formation of NO_2 from the reaction 'NO + O_3' in the sampling line was less than 0.01 % with respect to the ambient NO_2 concentrations. Line loss or photolysis of NO_2 was avoided by using PTFE lines (Polytetrafluoroethylene) covered with a dark insulating material. The average pressure inside the detection cell for the entire period of PARADE was 6.95 ± 0.27 (1σ) hPa. Several automated calibrations (2 - 8 per day) and background level measurements (once per hour) were conducted during PARADE to ensure the precision and accuracy of the instrument. Based on the hourly background level measurements, we established that the deviations for about 70 % (1 σ) of successive background signal measurements (no. of measurements > 500) were within an equivalent value of ± 8 ppt_v of NO_2. Any NO_2 impurity in the used zero air (hydrocarbon-free) would lead to under estimation of ambient NO_2 levels for PARADE and further contribute to the uncertainty. Nevertheless, previously describe deviations of 8 ppt_v in the background signal during PARADE could be a good indicator for this uncertainty. A malfunction of the O_3 generator occurred in the period 4 to 10 September that disturbed the GANDALF calibration system. A correction of 12 % is introduced for the period 4 – 10 September, based on the correlation of GANDALF with the CRDS instrument prior to 4 September. During the last few days of this period, an extra baffle was installed in GANDALF. The baffle can be inserted easily into the detection block of GANDALF without disturbing the alignment of the laser. The advantage of the baffle is that it reduces the background counts by ~50 % while decreasing sensitivity by less than 5 %. The overall correlation between GANDALF and the derived median NO_2 is R^2 = 0.99 as shown in panel B of Fig. 10. The measurements of GANDALF tend to be 3 % higher compared to the derived median values of NO_2. This overestimation of slope from unity compared to the derived median value is within the range of the instrument uncertainties. The overall relative uncertainty of GANDALF during PARADE was about 5 % + 11 ppt_v and it showed an exponentially increasing trend from a higher to lower concentrations of NO_2. This increasing trend is mainly driven by the error in the background measurements. The slope and y-intercept of the fit are 1.03 and 0.027 ppb_v with the absolute error of the fit being 0.006 and 0.01 ppb_v, respectively.

[18] Relative humidity in %

Generally, all instruments for NO_2 showed reasonable agreement with the derived median NO_2. Based on Fig. 10, GANDALF (+ 3 %), CRDS (+ 6 %) and LP-DOAS (+ 2 %) showed over-estimation compared to the derived median values while the data from CLD was about − 5 % and from CE-DOAS about − 8 % lower than the median values. The overall differences are within the experimental limitations and instrumental uncertainties. Results of the comparison between individual NO_2 measurements and the derived median NO_2 at different ranges of NO_2 mixing ratios are summarised in Table 3.

3.2 Ratio distribution of NO_2 measurements

Various measurements of trace gases, meteorological parameters, and photolysis frequencies during PARADE provided an opportunity to look for indications of systematic differences between NO_2 instruments. Ratios of the individual NO_2 measurements to GANDALF, which are referred to as "ratios" further in this section, are compared in respect of different atmospheric conditions. The distribution of ratios is shown as a histogram in the upper panel of Fig. 11 [A1, A2, A3, and A4] along their respective fits based on the normal distribution. The 'normal probability plot' for empirical probability versus ratios is shown in the lower panels [B1, B2, B3, and B4] of Fig. 11. This plot is a graphical representation of the normal distribution of ratios. The plot stays linear as long as the distributions are normal, and the deviation from the linear fit shows the divergence from the normal distribution. The solid line in the lower panels of Fig. 11 is between the 25^{th} and 75^{th} interquartile range of a ratio. The probability's grid (y-grid lines) is not linear and it is representative of the distance between quantiles of normal distribution.

The average, median, and standard deviations of ratios comparing GANDALF with other instruments are given in Table **4**. The variation in these ratios (CRDS/GANDALF, CE-DOAS/GANDALF, and CLD/GANDALF) is small compared to LP-DOAS/GANDALF. This is expected as the LP-DOAS is not an in situ technique and instead measures an average concentration along the light path. The ratios CRDS / GANDALF and LP-DOAS/GANDALF are close to unity, whereas in the case of CE-DOAS/GANDALF and CLD/GANDALF they deviate from unity by 0.15. All ratios distribution generally show a trend close to a normal distribution (Fig. 11 [A1, A2, A3, and A4]) but the skewness in LP-DOAS / GANDALF (A1 in Fig. 11) on both sides of the average value is relatively largest. In the lower panel of Fig. 11 [B1, B2, B3, and B4], the probabilities show a deviation from normality and a tail on top (towards the right) and bottom (towards the left) sides can be observed. The tail could be an indicator of outliers, caused by for example the non-normality of the precision at low values, background level, and potential interferences of NO_2 instruments. The lower panels [B1, B2, B3 and B4] of Fig. 11 show that a major fraction of the ratios is normally distributed, evident from the 25^{th} to 75^{th} interquartile range of probability in all cases. The percentile of probability towards normality is slightly greater (about 10^{th} to 90^{th} percentile) in the case of CLD/GANDALF compared to the others. The percentile is about 15^{th} to 80^{th} and 25^{th} to 90^{th} with (CRD/GANDALF, CE-DOAS/GANDALF) and (LP-DOAS/GANDALF), respectively. A perfect normal distribution should not be expected in these cases as mathematically a ratio between two normally distributed quantities does not follow a normal-distribution but it can be a distribution like the Cauchy-distribution (Weisstein, 2003). The long tails in the lower panel of Fig. 11 [B1, B2, B3, and B4] also indicates characteristics of the Cauchy distribution. In this type of distribution, the accuracy of average and standard deviation values cannot be increase by increasing the number of data points.

To identify systematic deviations based on other trace gases or parameters, ratios are further compared with the observed data of several trace gases, radiation, and meteorological parameters. There are only two cases, where a systematic correlation of ratios was observed with the observed quantities during PARADE, as shown in Fig. 12, and Fig. 13. In **Case 1**, ratios are presented as a function of the observed O_3 concentrations. The ratio between CLD and GANDALF shows a decreasing

trend with respect to an increase in the O_3 concentrations (subplot **C4**, Fig. 12). This ratio (CLD/GANDALF) averages 0.95 at levels less than 20 ppb_v O_3. It decreases to an average of 0.86 over the interval of 20 to 42 ppb_v O_3, while averaging 0.81 at levels above 42 ppb_v of O_3. There is no trend observed in other ratios (CRDS/GANDALF, LP-DOAS/GANDALF, and CE-DOAS/GANDALF) as shown in Fig. 12. The subplot (**C4**, Fig. 12) has been cross-checked by altering the GANDALF data in the denominator to the other three measurements (LP-DOAS, CRDS, and CE-DOAS) and qualitatively similar trends were observed as with GANDALF. The reason for this CLD/GANDALF trend is not clear at the moment. However, it seems that this trend may be an indirect impact due to the zero-air measurement of the CLD with the BLC unit ON which is dependent on the converter's history (exposition to ambient NO, NO_2, and HNO_3 concentrations along humidity) and potentially affect the ambient NO_2 measurements. So the dependency on O_3 might be an indirect effect: high ozone could point to transport from above with lower H_2O and lower NO_x, which both could affect the zero leading to an overestimation of the subtracted zero signal. In **Case 2** (subplot **D3**, Fig. 13), a correlation is observed for the ratio between CE-DOAS/GANDALF as a function of jNO_2. At higher values of jNO_2, the ratio approaches unity. The sampling line for CE-DOAS and CRDS was the same and no correlation for the ratio between CRDS and GANDALF is seen with respect to jNO_2. However, the data for the CRDS instrument was corrected for the effect of '$NO + O_3 \rightarrow NO_2$' in the sampling line and this correction for the CE-DOAS instrument was not implemented. Hence, the jNO_2 trend in the ratio could be indirectly from '$NO + O_3$'. A residence time of 10 s in the sampling line for the '$NO + O_3 \rightarrow NO_2$' reaction (using measured NO, and O_3) is sufficient to explain this trend. This correlation is also not observed for the ratios of LP-DOAS and CLD with respect to GANDALF. A cross check was done for panel D3 (Fig. 13) by exchanging GANDALF in the denominator to three other measurements (LP-DOAS, CRDS, and CLD); qualitatively similar trends were observed as previously. Besides the above-described systematic correlations, no indication of a potential interference is obtained for any of the instruments.

4 Summary

The laser-induced fluorescence based instrument (GANDALF) has been developed for the measurement of atmospheric NO_2. GANDALF has been tailored towards compact design with a low detection limit ($5 – 10$ ppt_v $1min^{-1}$), and high precision ($0.5\% + 3$ ppt_v $1min^{-1}$), making it capable of measuring NO_2 throughout the troposphere with a time resolution of 1 s to 1 min. The reliability of GANDALF was successfully tested during the PARADE-2011 field campaign. Several available NO_2 measurements based on different methods (absorption spectroscopy, chemiluminescence, and fluorescence) provided a unique chance of successful inter-comparison and most of the differences were under the uncertainties of individual measurements. The selectivity of NO_2 measurement with GANDALF compared to other measurements in ambient air was assessed during PARADE and no potential interference was found. This prototype could provide useful measurements of NO_2 under remote conditions where an interference-free detection is absolutely essential for the study of NO_x chemistry especially in the context of O_3 formation, and radical loss processes.

5 Acknowledgements

This work was done as a part of the first author's PhD, who is grateful for the constructive comments of Prof. P. Hoor during the PhD advisory committee meetings. The financial support from DFG (Deutsche Forschungsgemeinschaft) within the ''DFG-Verfahren: Schwerpunktprogramm, SPP 1294: Bereich Infrastruktur - Atmospheric and Earth system research with the "High Altitude and Long Range Research Aircraft" (HALO)'' is gratefully acknowledged. The authors are thankful to M. Tang, B.

Bohn, F. Berkes, and G. Phillips, for the data of NO_3/N_2O_5, jNO_2, H_2O, and $ClNO_2$, respectively. The acknowledgement extends to K. Hens, A. Novelli, E. Regelin, C.T. Ernest, C. Mallik for the useful comments/logistics, the site engineers, DWD (Germany's National Meteorological Service) for meteorological data, and to the Goethe University, Frankfurt, for use of the Taunus Observatory facilities.

6 References

Atkinson, R., Baulch, D. L., Cox, R. A., Crowley, J. N., Hampson, R. F., Hynes, R. G., Jenkin, M. E., Rossi, M. J., and Troe, J.: Evaluated kinetic and photochemical data for atmospheric chemistry: Volume I - gas phase reactions of O_x, HO_x, NO_x and SO_x species, Atmos Chem Phys, 4, 1461-1738, 2004.

Bekooy, J. P., Meerts, W. L., and Dymanus, A.: High-Resolution Laser-rf Spectroscopy on the $A^2\Pi_{3/2}$-$X^2\Pi_{3/2}$ System of Iodine Oxide (IO), J Mol Spectrosc, 102, 320-343, Doi 10.1016/0022-2852(83)90044-9, 1983.

Bonn, B., Bourtsoukidis, E., Sun, T. S., Bingemer, H., Rondo, L., Javed, U., Li, J., Axinte, R., Li, X., Brauers, T., Sonderfeld, H., Koppmann, R., Sogachev, A., Jacobi, S., and Spracklen, D. V.: The link between atmospheric radicals and newly formed particles at a spruce forest site in Germany, Atmos. Chem. Phys., 14, 10823-10843, 10.5194/acp-14-10823-2014, 2014.

Bradshaw, J., Davis, D., Crawford, J., Chen, G., Shetter, R., Muller, M., Gregory, G., Sachse, G., Blake, D., Heikes, B., Singh, H., Mastromarino, J., and Sandholm, S.: Photofragmentation two-photon laser-induced fluorescence detection of NO_2 and NO: Comparison of measurements with model results based on airborne observations during PEM-Tropics A, Geophys Res Lett, 26, 471-474, Doi 10.1029/1999gl900015, 1999.

Browne, E. C., and Cohen, R. C.: Effects of biogenic nitrate chemistry on the NO_x lifetime in remote continental regions, Atmos Chem Phys, 12, 11917-11932, DOI 10.5194/acp-12-11917-2012, 2012.

Burkholder, J. B., Talukdar, R. K., Ravishankara, A. R., and Solomon, S.: Temperature-Dependence of the HNO_3 UV Absorption Cross-Sections, J Geophys Res-Atmos, 98, 22937-22948, Doi 10.1029/93jd02178, 1993.

Butkovskaya, N., Kukui, A., and Le Bras, G.: HNO3 forming channel of the HO2+NOreaction as a function of pressure and temperature in the ranges of 72-600 torr and 223-323 K, J Phys Chem A, 111, 9047-9053, 10.1021/jp074117m, 2007.

Cantrell, C. A.: Technical Note: Review of methods for linear least-squares fitting of data and application to atmospheric chemistry problems, Atmos Chem Phys, 8, 5477-5487, 2008.

Cariolle, D., Evans, M. J., Chipperfield, M. P., Butkovskaya, N., Kukui, A., and Le Bras, G.: Impact of the new HNO(3)-forming channel of the HO(2)+NO reaction on tropospheric HNO(3), NO(x), HO(x) and ozone, Atmos Chem Phys, 8, 4061-4068, 2008.

Carpenter, L. J., Monks, P. S., Bandy, B. J., Penkett, S. A., Galbally, I. E., and Meyer, C. P.: A study of peroxy radicals and ozone photochemistry at coastal sites in the northern and southern hemispheres, J Geophys Res-Atmos, 102, 25417-25427, Doi 10.1029/97jd02242, 1997.

Clapp, L. J., and Jenkin, M. E.: Analysis of the relationship between ambient levels Of O_3, NO_2 and NO as a function of NO chi in the UK, Atmos Environ, 35, 6391-6405, Doi 10.1016/S1352-2310(01)00378-8, 2001.

Cleary, P. A., Wooldridge, P. J., and Cohen, R. C.: Laser-induced fluorescence detection of atmospheric NO_2 with a commercial diode laser and a supersonic expansion, Appl Optics, 41, 6950-6956, Doi 10.1364/Ao.41.006950, 2002.

Commane, R., Seitz, K., Bale, C. S. E., Bloss, W. J., Buxmann, J., Ingham, T., Platt, U., Pohler, D., and Heard, D. E.: Iodine monoxide at a clean marine coastal site: observations of high frequency variations and inhomogeneous distributions, Atmos Chem Phys, 11, 6721-6733, DOI 10.5194/acp-11-6721-2011, 2011.

Crawford, J., Davis, D., Chen, G., Bradshaw, J., Sandholm, S., Gregory, G., Sachse, G., Anderson, B., Collins, J., Blake, D., Singh, H., Heikes, B., Talbot, R., and Rodriguez, J.: Photostationary state analysis of the NO2-NO system based on airborne observations from the western and central North Pacific, J Geophys Res-Atmos, 101, 2053-2072, Doi 10.1029/95jd02201, 1996.

Crutzen, P. J.: Role of NO and NO_2 in the Chemistry of the Troposphere and Stratosphere, Annu Rev Earth Pl Sc, 7, 443-472, DOI 10.1146/annurev.ea.07.050179.002303, 1979.

Dari-Salisburgo, C., Di Carlo, P., Giammaria, F., Kajii, Y., and D'Altorio, A.: Laser induced fluorescence instrument for NO_2 measurements: Observations at a central Italy background site, Atmos Environ, 43, 970-977, 10.1016/j.atmosenv.2008.10.037, 2009.

Ehhalt, D. H., Rohrer, F., and Wahner, A.: Sources and distribution of NO_x in the upper troposphere at northern mid-latitudes Journal of Geophysical Research: Atmospheres (1984?2012) Volume 97, Issue D4, Journal of Geophysical Research: Atmospheres (1984-2012), 97, 3725-3738, 1992.

Fong, C., and Brune, W. H.: A laser induced fluorescence instrument for measuring tropospheric NO_2, Review of Scientific Instruments, 68, 4253, 10.1063/1.1148384, 1997.

Fontijn, A., Sabadell, A. J., and Ronco, R. J.: Homogeneous Chemiluminescent Measurement of Nitric Oxide with Ozone - Implications for Continuous Selective Monitoring of Gaseous Air Pollutants, Anal Chem, 42, 575-579, Doi 10.1021/Ac60288a034, 1970.

Ge, B. Z., Sun, Y. L., Liu, Y., Dong, H. B., Ji, D. S., Jiang, Q., Li, J., and Wang, Z. F.: Nitrogen dioxide measurement by cavity attenuated phase shift spectroscopy (CAPS) and implications in ozone production efficiency and nitrate formation in Beijing, China, J Geophys Res-Atmos, 118, 9499-9509, Doi 10.1002/Jgrd.50757, 2013.

George, L. A., and Obrien, R. J.: Prototype Fage Determination of NO_2, Journal of Atmospheric Chemistry, 12, 195-209, Doi 10.1007/Bf00048073, 1991.

Ghosh, B., Papanastasiou, D. K., Talukdar, R. K., Roberts, J. M., and Burkholder, J. B.: Nitryl Chloride ($ClNO_2$): UV/Vis Absorption Spectrum between 210 and 296 K and O(P-3) Quantum Yield at 193 and 248 nm, J Phys Chem A, 116, 5796-5805, Doi 10.1021/Jp207389y, 2012.

Gottschaldt, K., Voigt, C., Jockel, P., Righi, M., Deckert, R., and Dietmuller, S.: Global sensitivity of aviation NOx effects to the HNO3-forming channel of the HO2 + NO reaction, Atmos Chem Phys, 13, 3003-3025, 10.5194/acp-13-3003-2013, 2013.

Harwood, M. H., Jones, R. L., Cox, R. A., Lutman, E., and Rattigan, O. V.: Temperature-Dependent Absorption Cross-Sections of N_2O_5, J Photoch Photobio A, 73, 167-175, Doi 10.1016/1010-6030(93)90001-2, 1993.

Harwood, M. H., Burkholder, J. B., Hunter, M., Fox, R. W., and Ravishankara, A. R.: Absorption cross sections and self-reaction kinetics of the IO radical, J Phys Chem A, 101, 853-863, Doi 10.1021/Jp962429b, 1997.

Herndon, S. C., Shorter, J. H., Zahniser, M. S., Nelson, D. D., Jayne, J., Brown, R. C., Miake-Lye, R. C., Waitz, I., Silva, P., Lanni, T., Demerjian, K., and Kolb, C. E.: NO and NO_2 emission ratios measured from in-use commercial aircraft during taxi and takeoff, Environ Sci Technol, 38, 6078-6084, Doi 10.1021/Es049701c, 2004.

Herriott, D., Kompfner, R., and Kogelnik, H.: Off-Axis Paths in Spherical Mirror Interferometers, Appl Optics, 3, 523-&, Doi 10.1364/Ao.3.000523, 1964.

Hofzumahaus, A., Rohrer, F., Lu, K. D., Bohn, B., Brauers, T., Chang, C. C., Fuchs, H., Holland, F., Kita, K., Kondo, Y., Li, X., Lou, S. R., Shao, M., Zeng, L. M., Wahner, A., and Zhang, Y. H.: Amplified Trace Gas Removal in the Troposphere, Science, 324, 1702-1704, 10.1126/science.1164566, 2009.

Horowitz, A., Meller, R., and Moortgat, G. K.: The UV-VIS absorption cross sections of the alpha-dicarbonyl compounds: Pyruvic acid, biacetyl and glyoxal, J Photoch Photobio A, 146, 19-27, Doi 10.1016/S1010-6030(01)00601-3, 2001.

Hosaynali Beygi, Z., Fischer, H., Harder, H. D., Martinez, M., Sander, R., Williams, J., Brookes, D. M., Monks, P. S., and Lelieveld, J.: Oxidation photochemistry in the Southern Atlantic boundary layer: unexpected deviations of photochemical steady state, Atmos. Chem. Phys., 11, 8497-8513, 10.5194/acp-11-8497-2011, 2011.

Keller-Rudek, H., Moortgat, G. K., Sander, R., and Sörensen, R.: The MPI-Mainz UV/VIS Spectral Atlas of Gaseous Molecules of Atmospheric Interest, Earth Syst. Sci. Data, 5, 365-373, 10.5194/essd-5-365-2013, 2013.

Kubistin, D., Harder, H., Martinez, M., Rudolf, M., Sander, R., Bozem, H., Eerdekens, G., Fischer, H., Gurk, C., Klupfel, T., Konigstedt, R., Parchatka, U., Schiller, C. L., Stickler, A., Taraborrelli, D., Williams, J., and Lelieveld, J.: Hydroxyl radicals in the tropical troposphere over the Suriname rainforest: comparison of measurements with the box model MECCA, Atmos Chem Phys, 10, 9705-9728, DOI 10.5194/acp-10-9705-2010, 2010.

Land, D. V., Levick, A. P., and Hand, J. W.: The use of the Allan deviation for the measurement of the noise and drift performance of microwave radiometers, Measurement Science and Technology, 18, 1917-1928, 10.1088/0957-0233/18/7/018, 2007.

Lelieveld, J., and Crutzen, P. J.: Influences of Cloud Photochemical Processes on Tropospheric Ozone, Nature, 343, 227-233, Doi 10.1038/343227a0, 1990.

Lelieveld, J., Butler, T. M., Crowley, J. N., Dillon, T. J., Fischer, H., Ganzeveld, L., Harder, H., Lawrence, M. G., Martinez, M., Taraborrelli, D., and Williams, J.: Atmospheric oxidation capacity sustained by a tropical forest, Nature, 452, 737-740, 10.1038/nature06870, 2008.

Li, J. S., Reiffs, A., Parchatka, U., and Fischer, H.: In Situ Measurements of Atmospheric Co and Its Correlation with Nox and O-3 at a Rural Mountain Site, Metrol Meas Syst, 22, 25-38, 2015.

Logan, J. A.: Nitrogen-Oxides in the Troposphere - Global and Regional Budgets, J Geophys Res-Oc Atm, 88, 785-807, Doi 10.1029/Jc088ic15p10785, 1983.

Martinez, M., Harder, H., Kubistin, D., Rudolf, M., Bozem, H., Eerdekens, G., Fischer, H., Klupfel, T., Gurk, C., Konigstedt, R., Parchatka, U., Schiller, C. L., Stickler, A., Williams, J., and Lelieveld, J.: Hydroxyl radicals in the tropical troposphere over the Suriname rainforest: airborne measurements, Atmos Chem Phys, 10, 3759-3773, 2010.

Matsumi, Y., Murakami, S., Kono, M., Takahashi, K., Koike, M., and Kondo, Y.: High-sensitivity instrument for measuring atmospheric NO_2, Anal Chem, 73, 5485-5493, Doi 10.1021/Ac010552f, 2001.

Matsumoto, J., Hirokawa, J., Akimoto, H., and Kajii, Y.: Direct measurement of NO2 in the marine atmosphere by laser-induced fluorescence technique, Atmos Environ, 35, 2803-2814, Doi 10.1016/S1352-2310(01)00078-4, 2001.

Matsumoto, J., and Kajii, Y.: Improved analyzer for nitrogen dioxide by laser-induced fluorescence technique, Atmos Environ, 37, 4847-4851, 10.1016/j.atmosenv.2003.08.023, 2003.

Meller, R., Raber, W., Crowley, J. N., Jenkin, M. E., and Moortgat, G. K.: The Uv-Visible Absorption-Spectrum of Methylglyoxal, J Photoch Photobio A, 62, 163-171, Doi 10.1016/1010-6030(91)87017-P, 1991.

Molina, L. T., and Molina, M. J.: Ultraviolet-Absorption Spectrum of Chlorine Nitrite, Clono, Geophys Res Lett, 4, 83-86, Doi 10.1029/Gl004i002p00083, 1977.

Molina, L. T., and Molina, M. J.: Chlorine Nitrate Ultraviolet-Absorption Spectrum at Stratospheric Temperatures, J Photochem, 11, 139-144, Doi 10.1016/0047-2670(79)80047-7, 1979.

Mollner, A. K., Valluvadasan, S., Feng, L., Sprague, M. K., Okumura, M., Milligan, D. B., Bloss, W. J., Sander, S. P., Martien, P. T., Harley, R. A., McCoy, A. B., and Carter, W. P. L.: Rate of Gas Phase Association of Hydroxyl Radical and Nitrogen Dioxide, Science, 330, 646-649, 10.1126/science.1193030, 2010.

Monks, P. S.: Gas-phase radical chemistry in the troposphere, Chemical Society reviews, 34, 376-395, 10.1039/b307982c, 2005.

Newman, S. M., Howie, W. H., Lane, I. C., Upson, M. R., and Orr-Ewing, A. J.: Predissociation of the $A^2\Pi_{3/2}$ state of IO studied by cavity ring-down spectroscopy, J Chem Soc Faraday T, 94, 2681-2688, Doi 10.1039/A805103h, 1998.

Osthoff, H. D., Brown, S. S., Ryerson, T. B., Fortin, T. J., Lerner, B. M., Williams, E. J., Pettersson, A., Baynard, T., Dube, W. P., Ciciora, S. J., and Ravishankara, A. R.: Measurement of atmospheric NO_2 by pulsed cavity ring-down spectroscopy, J Geophys Res-Atmos, 111, Artn D12305
Doi 10.1029/2005jd006942, 2006.

Parra, J., and George, L. A.: Development of an ambient pressure laser-induced fluorescence instrument for nitrogen dioxide, Appl Optics, 48, 3355-3361, 2009.

Perner, D., and Platt, U.: Detection of Nitrous-Acid in the Atmosphere by Differential Optical-Absorption, Geophys Res Lett, 6, 917-920, Doi 10.1029/Gl006i012p00917, 1979.

Phillips, G. J., Tang, M. J., Thieser, J., Brickwedde, B., Schuster, G., Bohn, B., Lelieveld, J., and Crowley, J. N.: Significant concentrations of nitryl chloride observed in rural continental Europe associated with the influence of sea salt chloride and anthropogenic emissions, Geophys Res Lett, 39, Artn L10811
Doi 10.1029/2012gl051912, 2012.

Platt, U., Perner, D., and Patz, H. W.: Simultaneous Measurement of Atmospheric CH_2O, O_3, and NO_2 by Differential Optical-Absorption, J Geophys Res-Oc Atm, 84, 6329-6335, Doi 10.1029/Jc084ic10p06329, 1979.

Platt, U., and Stutz, J.: Differential Optical Absorption Spectroscopy, in, Springer-Verlag Berlin Heidelberg, 2008.

Platt, U., Meinen, J., Pohler, D., and Leisner, T.: Broadband Cavity Enhanced Differential Optical Absorption Spectroscopy (CE-DOAS) - applicability and corrections, Atmospheric Measurement Techniques, 2, 713-723, 2009.

Pöhler, D., Vogel, L., Friess, U., and Platt, U.: Observation of halogen species in the Amundsen Gulf, Arctic, by active long-path differential optical absorption spectroscopy, Proc Natl Acad Sci U S A, 107, 6582-6587, 10.1073/pnas.0912231107, 2010.

Reed, C., Evans, M. J., Di Carlo, P., Lee, J. D., and Carpenter, L. J.: Interferences in photolytic NO2 measurements: explanation for an apparent missing oxidant?, Atmos. Chem. Phys., 16, 4707-4724, 10.5194/acp-16-4707-2016, 2016.

Riley, W. J.: A test suite for the calculation of time domain frequency stability, Proceedings of the 1995 Ieee International Frequency Control Symposium, 360-366, Doi 10.1109/Freq.1995.483922, 1995.

Riley, W. J.: Handbook of Frequency Stability Analysis, National Institute of Standards and Technology (NIST), U.S. Department of Commerce, 136 pp., 2008.

Sander, S. P., Abbatt, J., Barker, J. R., Burkholder, J. B., Friedl, R. R., Golden, D. M., Huie, R. E., Kolb, C. E., Kurylo, M. J., Moortgat, G. K., Orkin, V. L., and and Wine, P. H.: Chemical Kinetics and Photochemical Data for Use in Atmospheric Studies, in: JPL Publication 10-6, 2011.

Sandholm, S. T., Bradshaw, J. D., Dorris, K. S., Rodgers, M. O., and Davis, D. D.: An Airborne Compatible Photofragmentation 2-Photon Laser-Induced Fluorescence Instrument for Measuring Background Tropospheric Levels of No, Nox, and No2, J Geophys Res-Atmos, 95, 10155-10161, DOI 10.1029/JD095iD07p10155, 1990.

Seinfeld, J. H., and Pandis, S. N.: Atmospheric Chemistry and Physics - From Air Pollution to Climate Change (2nd Edition), John Wiley & Sons, 2006.

Singer, R. J., Crowley, J. N., Burrows, J. P., Schneider, W., and Moortgat, G. K.: Measurement of the Absorption Cross-Section of Peroxynitric Acid between 210 and 330 nm in the Range 253-298-K, J Photoch Photobio A, 48, 17-32, Doi 10.1016/1010-6030(89)87086-8, 1989.

Staffelbach, T. A., Orlando, J. J., Tyndall, G. S., and Calvert, J. G.: The Uv-Visible Absorption-Spectrum and Photolysis Quantum Yields of Methylglyoxal, J Geophys Res-Atmos, 100, 14189-14198, Doi 10.1029/95jd00541, 1995.

Stavrakou, T., Muller, J. F., Boersma, K. F., van der A, R. J., Kurokawa, J., Ohara, T., and Zhang, Q.: Key chemical NOx sink uncertainties and how they influence top-down emissions of nitrogen oxides, Atmos Chem Phys, 13, 9057-9082, 10.5194/acp-13-9057-2013, 2013.

Taketani, F., Kawai, M., Takahashi, K., and Matsumi, Y.: Trace detection of atmospheric NO_2 by laser-induced fluorescence using a GaN diode laser and a diode-pumped YAG laser, Appl Optics, 46, 907-915, Doi 10.1364/Ao.46.000907, 2007.

Talukdar, R. K., Burkholder, J. B., Schmoltner, A. M., Roberts, J. M., Wilson, R. R., and Ravishankara, A. R.: Investigation of the Loss Processes for Peroxyacetyl Nitrate in the Atmosphere - UV Photolysis and Reaction with OH, J Geophys Res-Atmos, 100, 14163-14173, Doi 10.1029/95jd00545, 1995.

Thieser, J., Schuster, G., Schuladen, J., Phillips, G. J., Reiffs, A., Parchatka, U., Pöhler, D., Lelieveld, J., and Crowley, J. N.: A two-channel thermal dissociation cavity ring-down spectrometer for the detection of ambient NO2, RO2NO2 and RONO2, Atmos. Meas. Tech., 9, 553-576, 10.5194/amt-9-553-2016, 2016.

690 Thornton, J. A., Wooldridge, P. J., and Cohen, R. C.: Atmospheric NO_2: In situ laser-induced fluorescence detection at parts per trillion mixing ratios, Anal Chem, 72, 528-539, Doi 10.1021/Ac9908905, 2000.

Vandaele, A. C., Hermans, C., Fally, S., Carleer, M., Colin, R., Merienne, M. F., Jenouvrier, A., and Coquart, B.: High-resolution Fourier transform measurement of the NO_2 visible and near-infrared absorption cross sections: Temperature and pressure effects, J Geophys Res-Atmos, 107, Artn 4348
695 Doi 10.1029/2001jd000971, 2002.

Villena, G., Bejan, I., Kurtenbach, R., Wiesen, P., and Kleffmann, J.: Interferences of commercial NO2 instruments in the urban atmosphere and in a smog chamber, Atmospheric Measurement Techniques, 5, 149-159, DOI 10.5194/amt-5-149-2012, 2012.

Washenfelder, R. A., Langford, A. O., Fuchs, H., and Brown, S. S.: Measurement of glyoxal using an incoherent broadband cavity enhanced absorption spectrometer, Atmos. Chem. Phys., 8, 7779-7793, 10.5194/acp-8-7779-2008, 2008.

700 Wayne, R. P., Barnes, I., Biggs, P., Burrows, J. P., Canosamas, C. E., Hjorth, J., Lebras, G., Moortgat, G. K., Perner, D., Poulet, G., Restelli, G., and Sidebottom, H.: The Nitrate Radical - Physics, Chemistry, and the Atmosphere, Atmos Environ a-Gen, 25, 1-203, Doi 10.1016/0960-1686(91)90192-A, 1991.

Weisstein, E. W.: CRC concise encyclopedia of mathematics, 2nd ed., Chapman & Hall/CRC, Boca Raton, 3242 p. pp., 2003.

Wojtas, J., Stacewicz, T., Bielecki, Z., Czyzewski, A., and Nowakowski, M.: NO_2 monitoring setup applying cavity enhanced
705 absorption spectroscopy, Eurocon 2007: The International Conference on Computer as a Tool, Vols 1-6, 2152-2154, 2007.

York, D., Evensen, N. M., Martinez, M. L., and Delgado, J. D.: Unified equations for the slope, intercept, and standard errors of the best straight line, American Journal of Physics, 72, 367-375, Doi 10.1119/1.1632486, 2004.

Atmos. Meas. Tech. Discuss., https://doi.org/10.5194/amt-2018-204
Manuscript under review for journal Atmos. Meas. Tech.
Discussion started: 5 July 2018

Atmospheric Measurement Techniques Discussions

7 Tables

Table 1: Overview of different LIF instruments

Reference	$\lambda^{laser\ type}$ (nm)	Laser power (mW)	Absorption cross-section ($\times 10^{-19}$) cm^2 molecule^{-1}	Cell pressure (Pa)	LOD (ppt$_v$ min^{-1})
(George and Obrien, 1991)	532 [1]	250	1.5	37	600
(Fong and Brune, 1997)	565 [2]	250	0.6	1000	460
(Thornton et al., 2000)	585 [3]	100-400	1	467	6
(Matsumi et al., 2001)	440 [4]	100	7	35	12
(Matsumoto et al., 2001)	523.5 [5]	360	1.4	93	125
(Cleary et al., 2002)	640.2 [6]	16	3.9 [C]	27	145
(Matsumoto and Kajii, 2003)	532 [7]	6500	1.5	267	4
(Taketani et al., 2007)	410 [8], 473 [9]	10, 15	6, 3	67	390, 140
(Parra and George, 2009)	406.3 [10]	35	6	Ambient	2000 [A]
(Dari-Salisburgo et al., 2009)	532 [11]	8000-12000	1.5	60	12
GANDALF	447- 450 [12]	Max. 200	5.3 [E]	700	5-10

[E] Effective absorption cross-section; [C] Cooling enhancement; [A] Ambient pressure in the detection cell.

Laser type (Table 1 column 2**)**

[1] Nd: YAG laser; [2] Copper vapour laser-pumped dye laser; [3] Pulsed YAG-pumped dye laser; [4] Optical parametric oscillator laser; [5] Nd: YLF laser harmonic; [6] External-cavity tunable diode laser; [7] Nd:YVO_4 pulse laser pumped by a solid-state laser; [8] GaN-based laser diode; [9] Diode-pumped Nd:YAG laser; [10] CW GaN semiconductor laser diode; [11] YAG Q-switched intra-cavity doubled laser; [12] CW diode laser

Table 2: NO_2 instruments located or sampling at the top of the platform during PARADE-2011.

Measurement (Operator)	Technique	Uncertainty	Detection Limit	Time resolution
LP-DOAS (IUP-HD)	Long Path DOAS	2 %	-	-
CE-DOAS (IUP-HD)	Cavity-Enhanced DOAS	5 - 10 %	300 ppt$_v$	30 s
CRDS (MPIC)	Cavity Ring-Down Spectrometer	6 % ; 20 ppt$_v$	50 ppt$_v$ (4s, 2σ)	4 s
CLD (BLC) (MPIC)	Chemiluminescence Detector/ Blue light convertor	105 ppt$_v$; 10 %	55 ppt$_v$ (2 s, 1σ)	2 s
GANDALF (MPIC)	Laser-Induced Fluorescence	5 % + 11 ppt$_v$ (1σ)	5 - 10 ppt$_v$ (1 min, SNR = 2)	1 s

Atmos. Meas. Tech. Discuss., https://doi.org/10.5194/amt-2018-204
Manuscript under review for journal Atmos. Meas. Tech.
Discussion started: 5 July 2018

Atmospheric Measurement Techniques Discussions

Table 3: Fit parameters based on the bivariate model function according to the relation (NO_2Instruments = a × [MedianNO_2] + b) at different NO_2 ranges. The value of NO_2Instruments-intercept 'b' is in ppb_v. 'N' is number of data points and R^2 is the square correlation coefficient.

NO_2 Instruments	a	± δ_a	b	± δ_b	N	R^2	a	± δ_a	b	± δ_b	N	R^2
	NO_2 < 1ppb$_v$						NO_2 ≥ 1 to ≤ 6 ppb$_v$					
LP-DOAS	1.23	0.07	-0.15	0.05	208	0.80	1.03	0.008	-0.03	0.01	964	0.90
CE-DOAS	0.95	0.06	-0.06	0.05	208	0.80	0.92	0.01	-0.03	0.02	964	0.99
CRDS	1.1	0.07	-0.02	0.05	208	0.83	1.06	0.01	0.002	0.02	964	0.99
CLD	0.99	0.08	-0.12	0.06	208	0.73	0.97	0.01	-0.13	0.02	964	0.98
GANDALF	1.06	0.07	0.015	0.05	208	0.74	1.04	0.01	0.015	0.02	964	0.99
	NO_2 > 6 to < 12 ppb$_v$						NO_2 ≥ 12 ppb$_v$					
LP-DOAS	1.2	0.08	-1.51	0.6	52	0.64	1.42	0.2	-6.64	4	15	0.69
CE-DOAS	0.91	0.09	0.075	0.7	52	0.94	0.87	0.2	0.55	3	15	0.96
CRDS	1.09	0.09	-0.16	0.6	52	0.94	1.04	0.2	0.38	3	15	0.94
CLD	1.02	0.1	-0.64	0.7	52	0.81	0.89	0.2	0.51	3	15	0.84
GANDALF	1.05	0.08	0.016	0.6	52	0.94	0.99	0.2	0.52	3	15	0.94

725

Table 4: The average values for ratios during PARADE.

Ratio	Average	Standard Deviation
LP-DOAS / GANDALF	0.96	0.19
CRDS / GANDALF	1.01	0.06
CE-DOAS / GANDALF	0.86	0.07
CLD / GANDALF	0.85	0.09

Atmos. Meas. Tech. Discuss., https://doi.org/10.5194/amt-2018-204
Manuscript under review for journal Atmos. Meas. Tech.
Discussion started: 5 July 2018

8 Figures

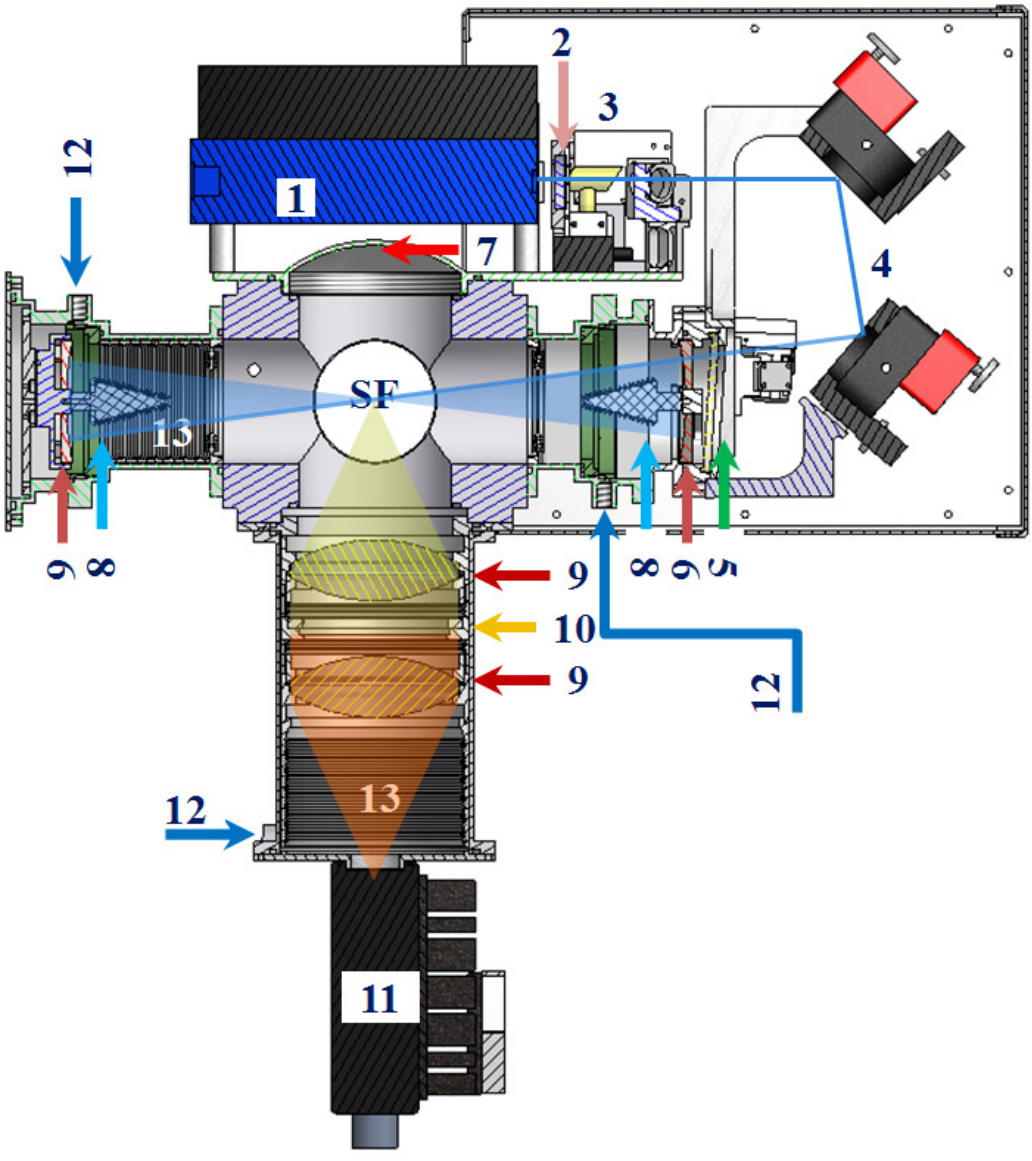

Figure 1: Section view[19] of GANDALF

730 **(SF)**: Sampling flow **(1):** Diode laser **(2):** Focussing lens **(3):** Optical reference system **(4):** Motorised mirrors **(5):** Laser entrance window with wedge **(6):** Herriott cell's mirrors **(7):** Concave mirror **(8):** Conical baffles **(9):** Focusing lens **(10):** Optical filters **(11):** PMT **(12):** Flushing for optics **(13):** Surfaces for reduction of the scatter

[19] Section view is based on Inventor-2009: The figure is created by defining a plane used to cut through the whole assembly. 3D AutoCAD models for the diode laser (1) by courtesy of Omicron Laserage Laserprodukte GmbH and beam splitter holder by courtesy of Newport.

Atmos. Meas. Tech. Discuss., https://doi.org/10.5194/amt-2018-204
Manuscript under review for journal Atmos. Meas. Tech.
Discussion started: 5 July 2018

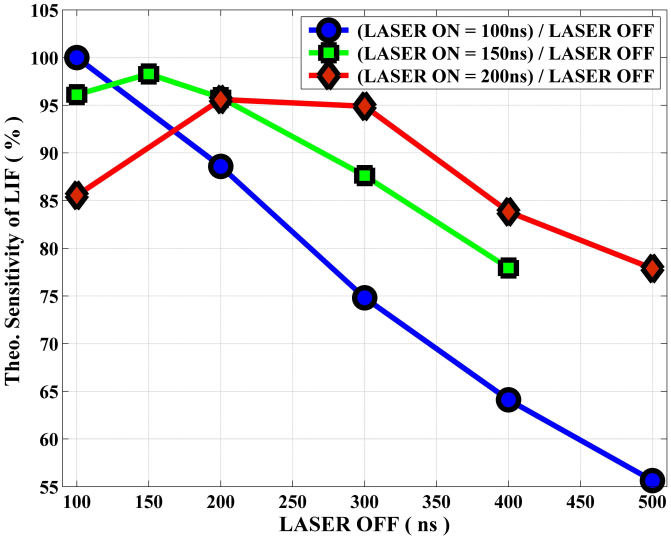

735 **Figure 2: Relative sensitivity of the instrument based on simulation is demonstrated for three different on/off cycles of diode laser operation.**

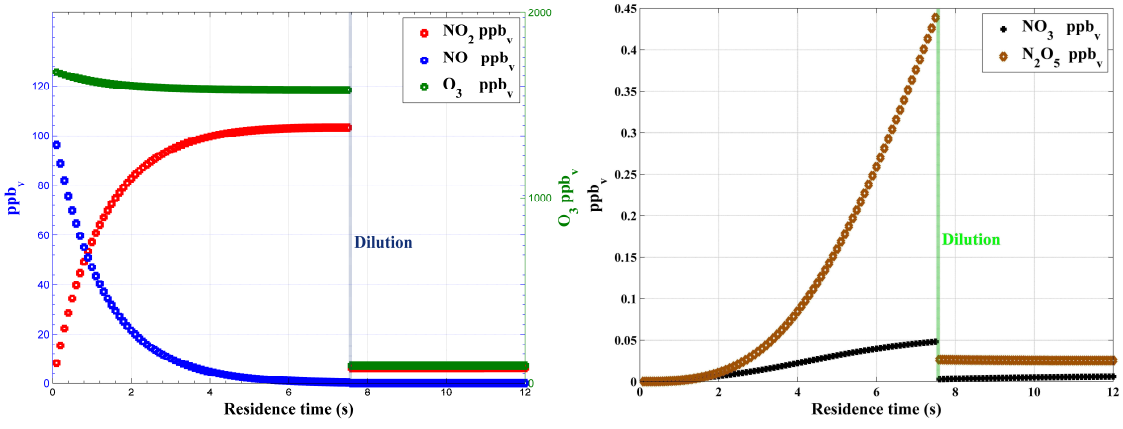

740 **Figure 3: Box model simulation of gas phase titration of NO and O_3 (left panel) with loss of NO_2 due to formation of NO_3 and N_2O_5 (right panel).**

745

Atmos. Meas. Tech. Discuss., https://doi.org/10.5194/amt-2018-204
Manuscript under review for journal Atmos. Meas. Tech.
Discussion started: 5 July 2018

Atmospheric Measurement Techniques Discussions

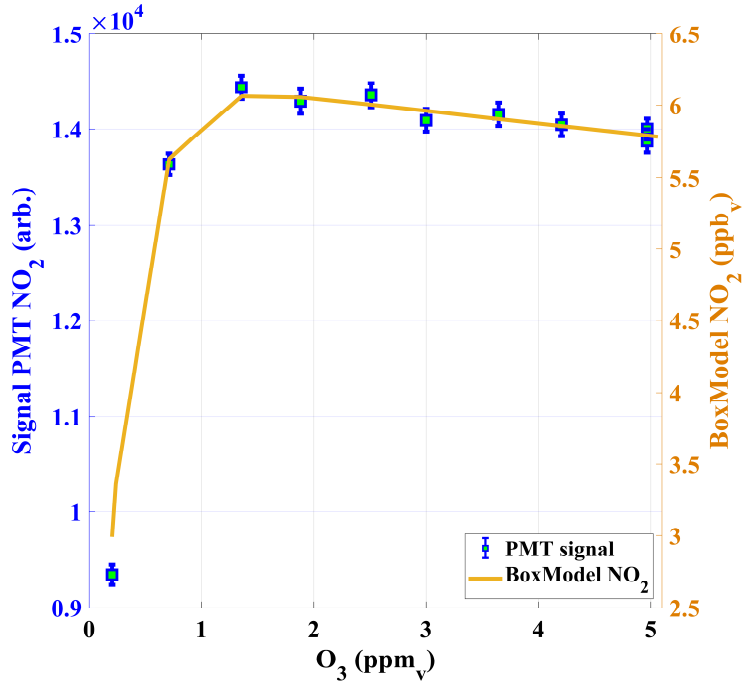

Figure 4: NO_2 signal as a function of O_3 in the calibrator.

750

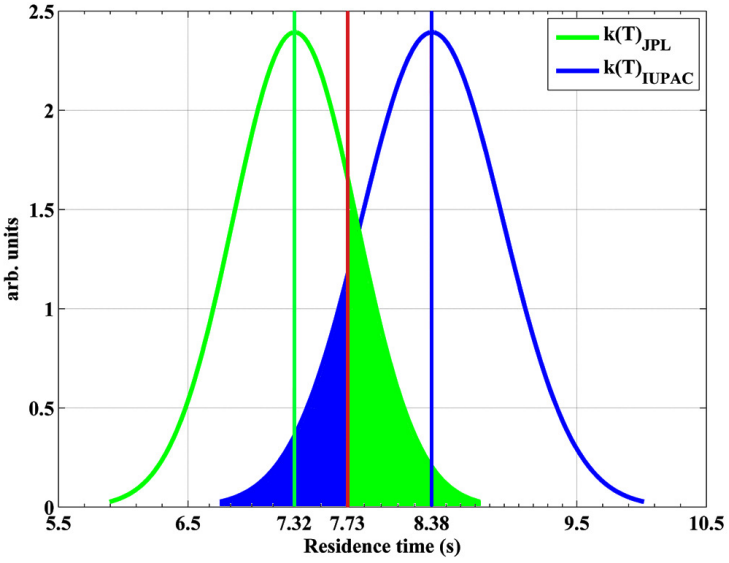

Figure 5: Residence time for NO_2 calibration gas in the calibrator based on Eq. 3. Also theoretically calculated residence time (7.73 s) is shown. The likelihoods (green or blue shaded areas) of residence times based on the JPL or IUPAC rate constant for being accurate are indistinguishable in comparison to the theoretically calculated residence time.

755

Atmos. Meas. Tech. Discuss., https://doi.org/10.5194/amt-2018-204
Manuscript under review for journal Atmos. Meas. Tech.
Discussion started: 5 July 2018

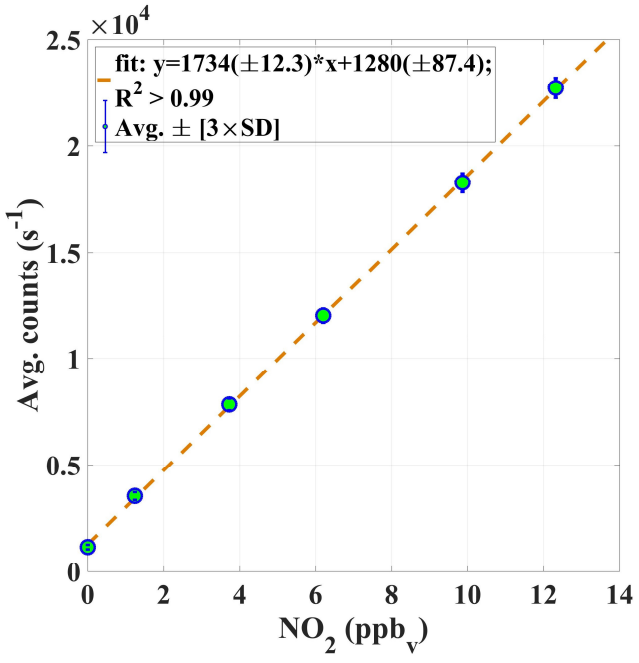

Figure 6: An example of the calibration signal vs known mixing ratios of NO_2. The calibration constant α_c (Eq. 1) is given by the slope of the curve.

760

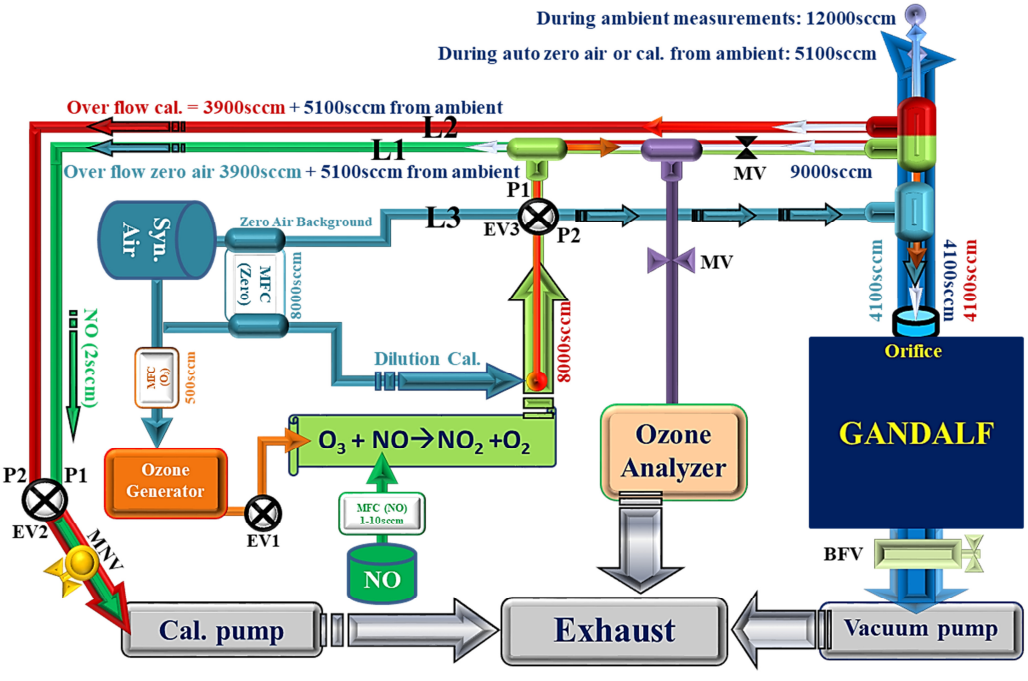

Figure 7: Schematic setup for automated calibrations during outdoor operations.

Atmos. Meas. Tech. Discuss., https://doi.org/10.5194/amt-2018-204
Manuscript under review for journal Atmos. Meas. Tech.
Discussion started: 5 July 2018

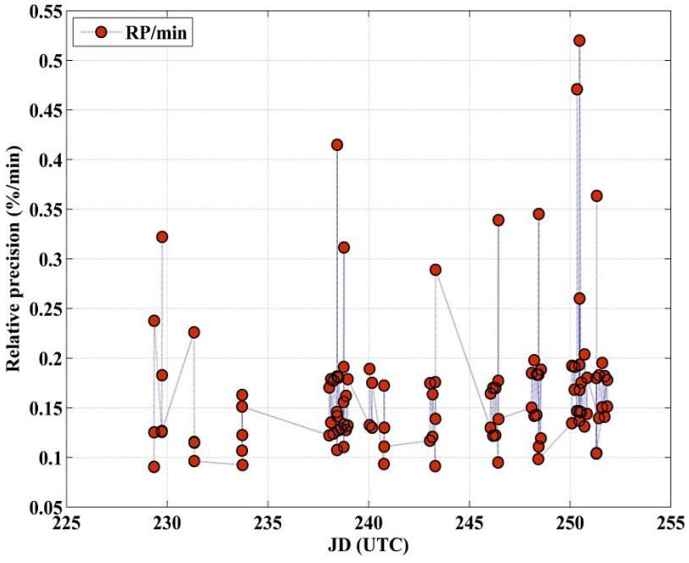

765 **Figure 8: Relative precision check of GANDALF for randomly selected NO_2 calibration points for different days (JD).**

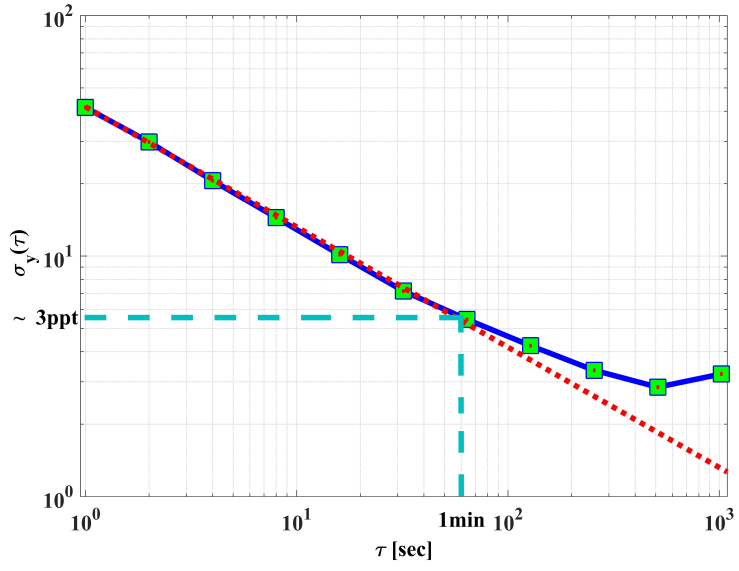

770 **Figure 9: An overlapping Allan deviation plot for the dependence of the 1σ variation in the background signal vs. integration time. The red colour dotted line shows the square root dependency of the signal.**

Atmos. Meas. Tech. Discuss., https://doi.org/10.5194/amt-2018-204
Manuscript under review for journal Atmos. Meas. Tech.
Discussion started: 5 July 2018

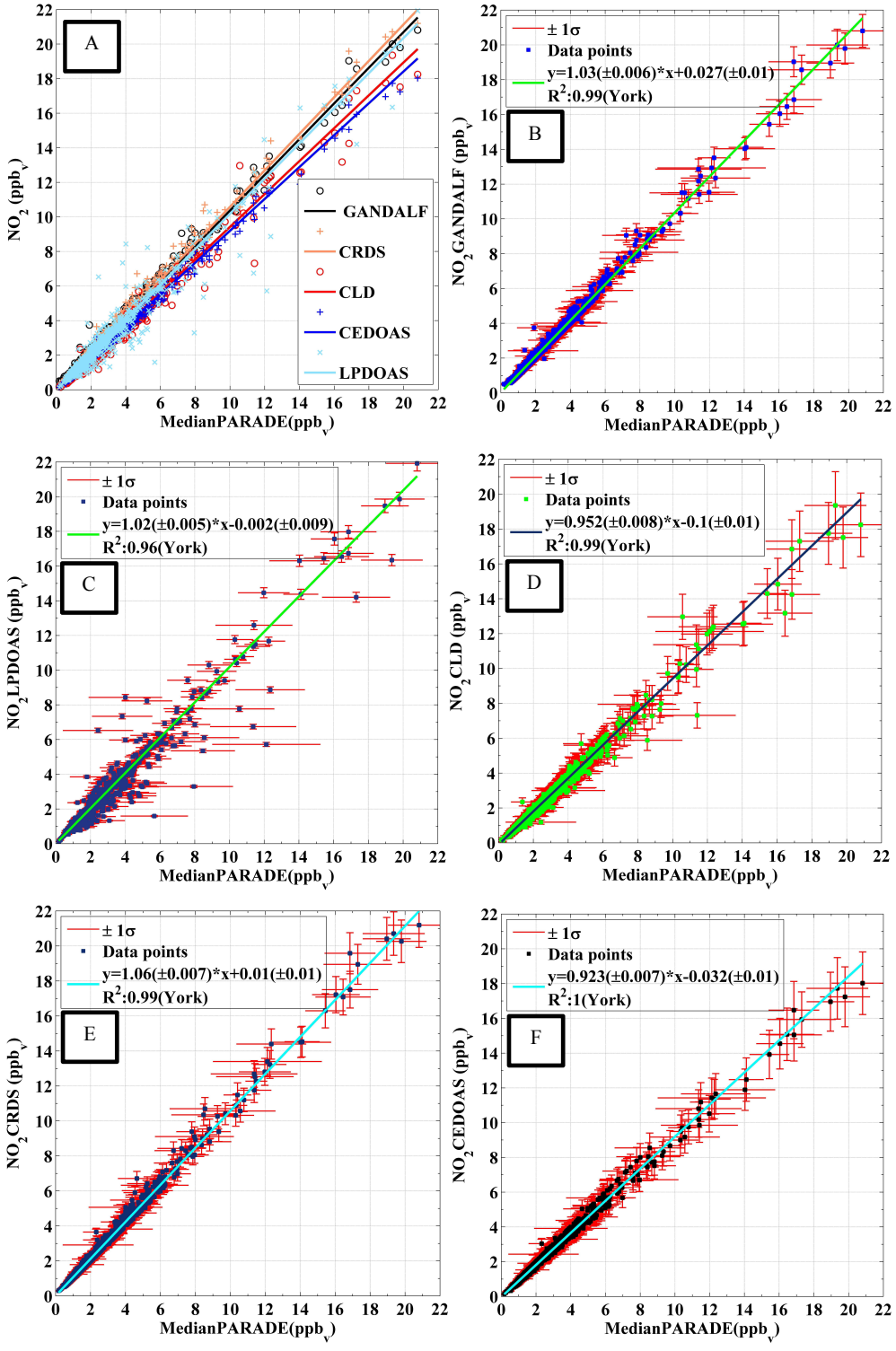

775

Figure 10: Correlation plots of individual NO_2 measurement versus the derived median values of all NO_2 measurement at the platform during PARADE. [A]: Overall, [B]: GANDALF, [C]: CLD, [D]: CRDS, [E]: LP-DOAS, [F]: CE-DOAS

Atmos. Meas. Tech. Discuss., https://doi.org/10.5194/amt-2018-204
Manuscript under review for journal Atmos. Meas. Tech.
Discussion started: 5 July 2018

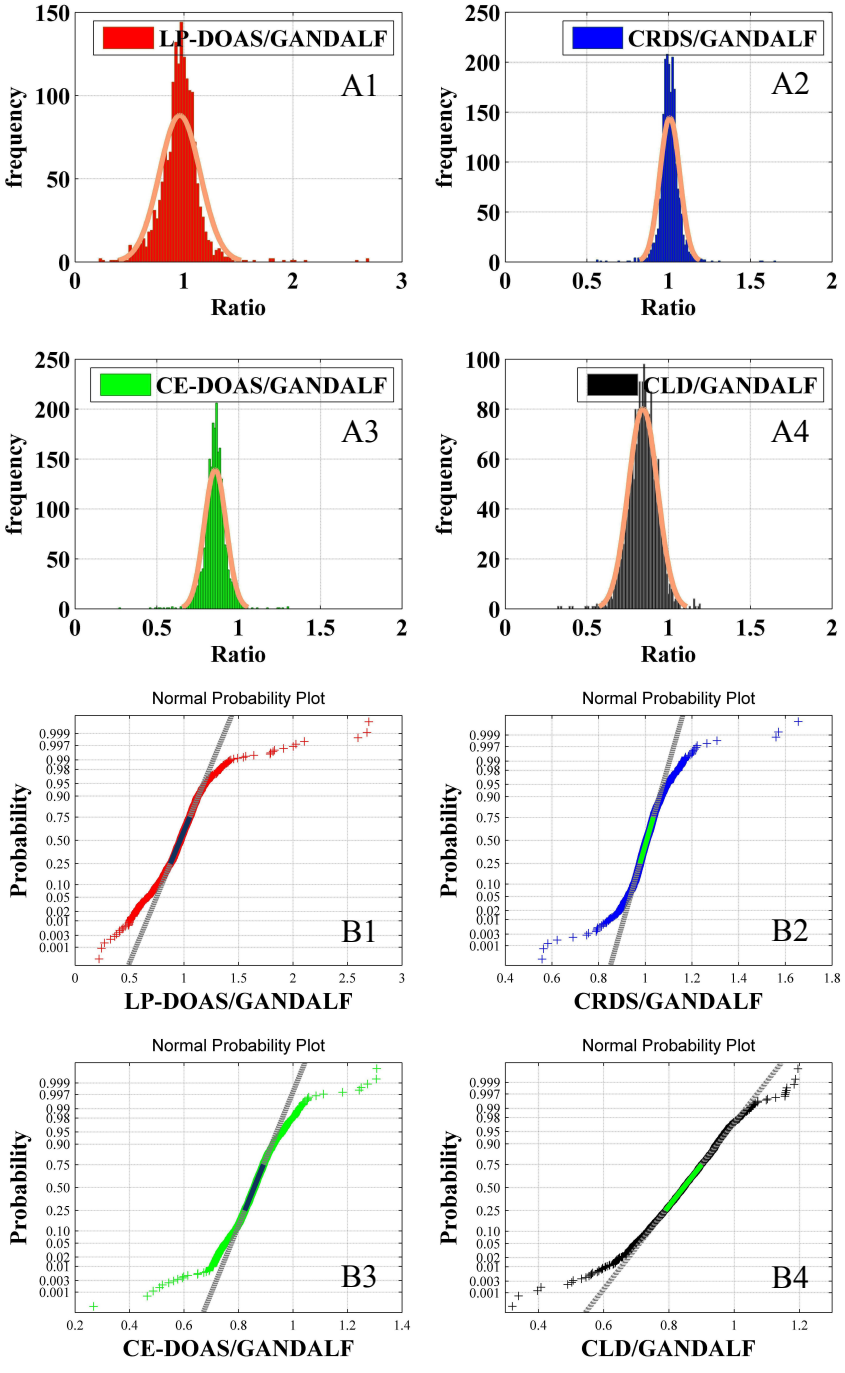

5 **Figure 11: Distribution of comparative instrument ratios is shown in upper panels (A1→A4) and a normal probability plot for comparative instrument ratios is shown in lower panels (B1→B4).**

Atmos. Meas. Tech. Discuss., https://doi.org/10.5194/amt-2018-204
Manuscript under review for journal Atmos. Meas. Tech.
Discussion started: 5 July 2018

Atmospheric Measurement Techniques Discussions

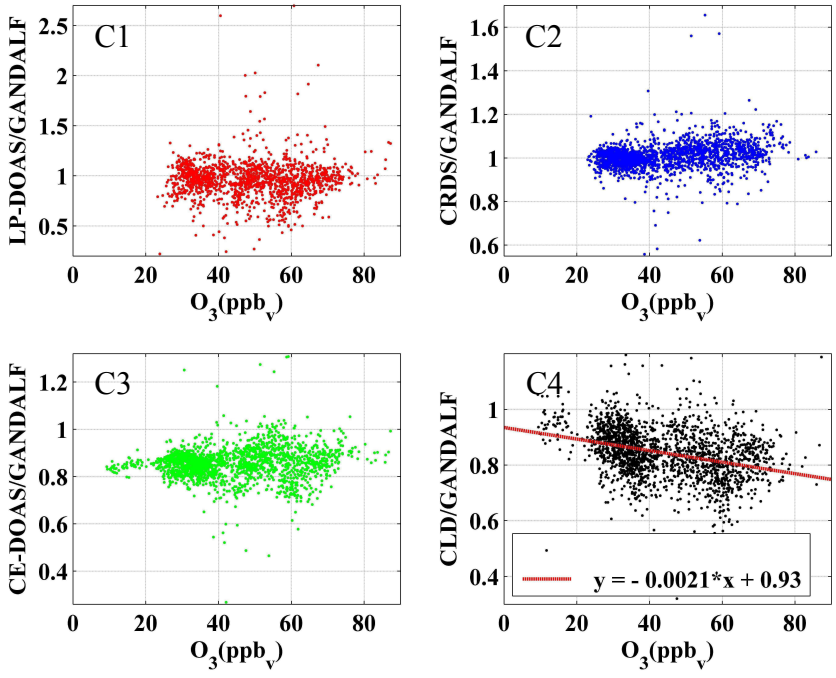

Figure 12: Ratios as a function of ambient O_3 during PARADE.

5

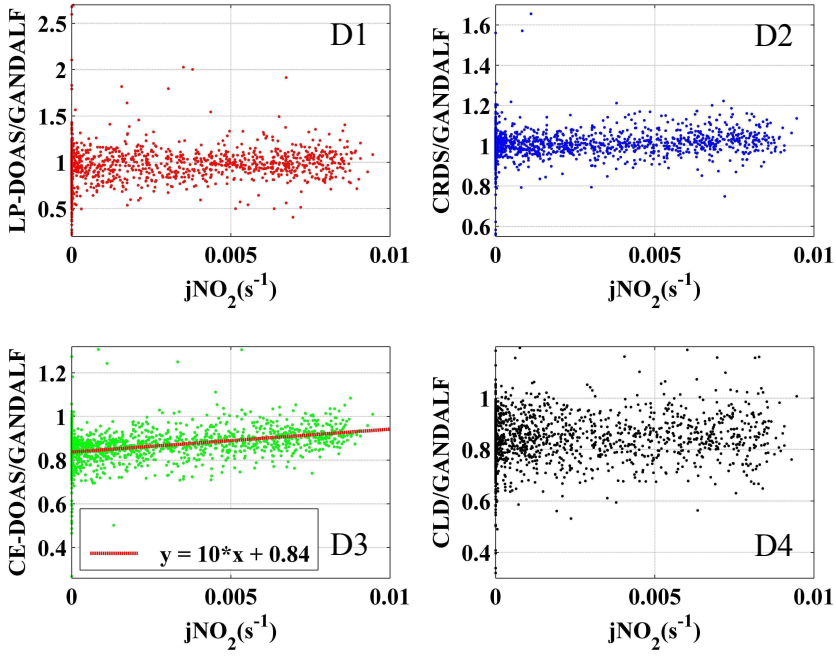

Figure 13: Ratios as a function of measured jNO_2 during PARADE.